nature communications

Article

https://doi.org/10.1038/s41467-025-64694-3

Single-molecule methods for characterizing receptor dimers reveal metastable opioid receptor homodimers that induce functional modulation

Received: 22 August 2024

Accepted: 23 September 2025

Peng Zhou[1] ✉, **Taka A. Tsunoyama**[1], **Rinshi S. Kasai**[2,3,4], **Koichiro M. Hirosawa**[3], **Ziya Kalay**[5], **Amine Aladag**[1], **Takahiro K. Fujiwara**[5], **Tatsushi Yokoyama**[6], **Masayuki Sakamoto**[6], **Ryoji Kise**[7], **Masataka Yanagawa**[7], **Asuka Inoue**[7], **Simone Pigolotti**[8] & **Akihiro Kusumi**[1,5] ✉

Opioid receptors (ORs) are critical for endogenous and synthetic analgesics. OR homodimerization is considered important for their pharmacological diversity, but whether they form homodimers remains controversial. Here, we establish that the three classical ORs, μ-, κ-, and δ-ORs (MOR, KOR, and DOR, respectively) undergo repeated transient (120-180 ms) homodimerizations every few seconds. This is achieved by using single-molecule imaging and developing theories for analyzing single-molecule colocalization data, which provide key parameters, such as homodimer-monomer dissociation equilibrium constants and rate constants. Their 9-26 amino-acid C-terminal cytoplasmic domains, without sequence similarities, are involved in specific homodimerization, whereas the transmembrane domains provide less specific affinities. Using the membrane-permeable peptides mimicking the C-terminal homodimerization sequences which block homodimerizations, functions of monomers and homodimers were dissected. KOR and DOR homodimers, but not MOR homodimers, activate downstream G-proteins differently from monomers upon agonist addition, without influencing OR internalization. These findings guide strategies to enhance OR-based analgesia.

Three classical opioid receptors (ORs), μ-, κ-, and δ-ORs (MOR, KOR, and DOR, respectively), are distributed across the central and peripheral nervous systems and play important roles in regulating pain perception, hedonic homeostasis, mood, and well-being[1,2]. ORs are prototypical class A G-protein-coupled receptors (GPCRs), and serve as key receptors for a variety of endogenous and synthetic analgesics. These OR subtypes play critical roles in pain therapeutics, and at the same time, in the development of tolerance to and dependence on

---

[1]Membrane Cooperativity Unit, Okinawa Institute of Science and Technology Graduate University, Onna-son, Okinawa 904-0495, Japan. [2]Division of Advanced Bioimaging, National Cancer Center Research Institute, Tokyo 104-0045, Japan. [3]Institute for Glyco-core Research (iGCORE), Gifu University, Gifu 501-1193, Japan. [4]Institute for Life and Medical Sciences, Kyoto University, Kyoto 606-8507, Japan. [5]Institute for Integrated Cell-Material Sciences (WPI-iCeMS), Kyoto University, Kyoto 606-8501, Japan. [6]Graduate School of Biostudies, Kyoto University, Kyoto 606-8501, Japan. [7]Graduate School of Pharmaceutical Sciences, Kyoto University, Kyoto 606-8501, Japan. [8]Biological Complexity Unit, Okinawa Institute of Science and Technology Graduate University, Onna-son, Okinawa 904-0495, Japan. ✉e-mail: zp19821001@gmail.com; akihiro.kusumi@oist.jp

analgesics, which are likely associated with activations of the inhibitory G-protein and β-arrestin pathways in complex manners[2–4].

The diversity of OR conformations and their interactions with other proteins not only drives various cellular physiological responses but also contributes to a spectrum of brain circuit responses, both beneficial and adverse[4–7]. Hence, a profound understanding of the mechanisms by which ORs' distinct downstream responses are induced is essential for the development of analgesic drugs with minimized side effects. In addition, receptor dimerization and clustering are often key steps for triggering the downstream signaling cascades in other receptor signaling pathways[8].

The pharmacological diversity of ORs might be enhanced by their propensity to form homodimers[9,10] and heterodimers[11–13]. Agonist-induced homodimer formation significantly influences the balance of MOR's downstream G-protein and β-arrestin pathways[14]. Other studies have suggested that dimerization, both homo and hetero, might modulate or be modulated by biased agonism, highlighting its significance in receptor signaling (see Refs. 15,16 for homodimers and Refs. 17,18 for heterodimers). For the β2-adrenergic receptor, another class A GPCR, homodimers are responsible for generating the basal receptor signal in the absence of agonists, a key common characteristic of GPCRs[19]. Furthermore, OR heterodimerization is important for their cooperative functions, as supported by functional and pharmacological studies[17,20]. Therefore, understanding both the homo- and hetero-dimerizations of ORs, as well as those of other class-A GPCRs, is fundamental to deciphering their functional regulation mechanisms[16,21–25].

Despite such extensive research, the very existence of homo- and hetero-dimers of ORs, particularly at various expression levels, remains controversial: our knowledge of OR expression levels under various physiological and pathological conditions and that on their local densities in distinct plasma membrane (PM) domains is quite limited[26–32]. Previous detection of homodimers of DOR[9,33,34], MOR[13,34], and KOR[13,34], and heterodimers of all OR pairs[34] contrasts with recent single-molecule imaging (SMI) studies. These SMI studies, performed at low expression levels in the PM of living cells, in contrast to the results that relied on much higher cellular expression levels or very high concentrations in vitro (conditions are often required for bulk observation methods), showed that MOR[27,35], DOR[35], and KOR[36] are predominantly monomeric. Therefore, they concluded that previously observed dimerization and its functional and pharmacological consequences would be artifacts due to the employment of very high OR concentrations. Meanwhile, other single-molecule investigations detected the nanodomains of KOR and MOR[37] as well as the transient MOR dimerization[28], which occurred only after DAMGO binding but not with morphine[14].

To address the issue of expression levels and resolve these controversies, determining the dimer-monomer equilibrium constant K_D is imperative, as it is unaffected by the expression levels. In addition, since several GPCR homodimers are apparently metastable with lifetimes on the order of 0.1–1 s[19,21,28,38–41], estimating the dimer dissociation and association rate constants, k_{off} and k_{on}, respectively, is essential for establishing the comprehensive description of the dynamic dimer-monomer equilibrium of ORs. Such insights would enable us to unequivocally determine whether ORs form homo- and hetero-dimers and to what extent at various local number densities, in different regions within the PM and in diverse cells in various brain regions.

More generally, studies of the molecular interactions and dimerizations of membrane molecules, which are critically important for understanding receptor signaling and signal transduction in the PM, are seriously hampered by the lack of methods to evaluate three fundamental constants, K_D, k_{off}, and k_{on}. To our knowledge, only two publications exist in the literature that reported all three thermodynamic and kinetic parameters (both happened to study GPCRs)[35,41]. However, the method we developed to measure K_D for the first time ever was cumbersome, and all single-molecule methods for measuring k_{off}, including ours, lacked mathematical rigor.

In the present research, we propose theoretical methods to address this issue, so that investigations of molecular interactions and dimerization in the PM can become more quantitative, which would greatly advance the field. We developed two theories, leading to two methods: one to evaluate k_{off} from the distribution of single-molecule colocalization durations (instead of intuitive methods employed previously), and another to estimate K_D from pair cross-correlation functions, which is much simpler than the previous method and more sensitive due to the use of a correlation method (with k_{on} calculated as k_{off}/K_D).

We present our findings in two back-to-back papers. This paper focuses on the development of single-molecule methods to evaluate three thermodynamic and kinetic constants describing molecular interactions and dimerization, which are then applied to OR homodimerization and dimer functions, while the companion paper addresses OR heterodimers and their functions[42].

In this study, we report that all three ORs engage in continual, repeated, transient homodimerizations at 37 °C, with K_Ds of 6.04 ± 0.57, 15.47 ± 1.54, and 16.62 ± 0.53 copies/μm^2 for KOR, MOR, and DOR, respectively. The homodimer lifetimes are in the range of 120−180 ms (dimer dissociation rate constants in the range of 6.71 to 8.47 s^{-1}), unequivocally demonstrating that even at expression levels as low as <1 copy/μm^2, the three ORs form transient homodimers. Furthermore, we identified that the ≈9–26 amino acid sequences in the cytoplasmic C-terminal domains, without sequence similarities, are involved in the distinct homodimerizations of the three ORs, in line with the previous DOR homodimerization data[9], whereas the transmembrane domains might promote both homo- and heterodimerizations in a less specific manner, in partial agreement with previous results[21,43–46]. Building on these amino-acid sequences, we developed peptides that suppress OR homodimerization within live cells. This has allowed us to distinguish the functions of OR dimers from monomers, which could not be done before. OR monomerization by these peptides enhances and diminishes agonist-induced signals downstream from G proteins for KOR and DOR, respectively, without influencing agonist-induced internalization. Meanwhile, monomerization had no discernible effect on MOR signaling or internalization. These findings may inform novel strategies in developing more effective and safer pain treatments.

Results

All three ORs continually interconvert between transient homodimers and monomers: analysis by colocalization index based on the pair cross-correlation function (PCCF)

ORs conjugated with the SNAPf tag protein at their N-termini (SNAPf-ORs; see Supplementary Data 1) were expressed in the PM of CHO-K1 cells, which do not express ORs[47]. These tagged ORs retained the same functionality as the non-tagged receptors (Supplementary Fig. 1a–d), were fluorescently labeled with SNAP-Surface 549 and SNAP-CF660R with 66% and 61% efficiencies, respectively (Supplementary Fig. 1e–g). Since these efficiencies were determined using quite different transmembrane proteins, we assume that they are applicable to all SNAPf-tagged proteins used in this work. For the experiments examining OR homodimerization, we simultaneously labeled a SNAPf-OR (for example, SNAPf-KOR) with both SNAP-Surface 549 and SNAP-CF660R so that the number densities of the two probes on the PM were about the same, with spot densities of 0.5 ± 0.25 spots/μm^2 for each color (total spot number densities of 1.0 ± 0.5 spots/μm^2; for conciseness, we will describe as ≈1 spot/μm^2 throughout this report), and then performed simultaneous dual-color single-molecule observations at normal video rate (30 Hz) at 37 °C, using a home-built total internal reflection fluorescence (TIRF) microscope[48,49].

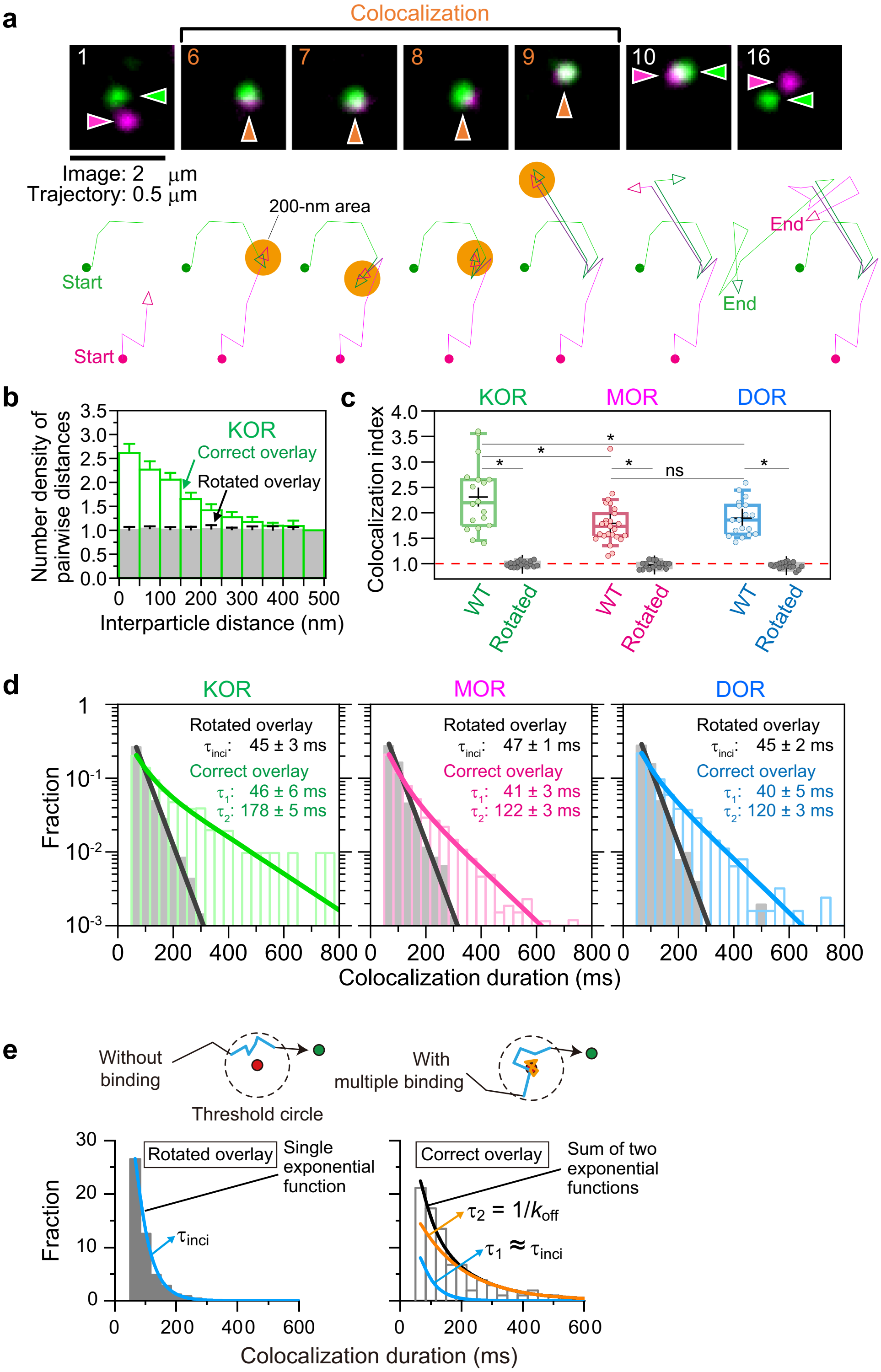

Almost all of the SNAPf-OR fluorescent spots (90-95%) exhibited simple Brownian diffusion in the PM by the criteria described previously[50], but in addition, they often exhibited temporary colocalization and co-diffusion[41], suggesting the frequent formation of transient homodimers (Supplementary Movies 1 and 2; Fig. 1a). We focused on simultaneous two-color experiments, due to the ease of image analysis. For the single-color imaging data, see Supplementary Fig. 2a and b, which show an example of repeated homodimerizations of a KOR molecule with different partner KOR molecules, consistent with the observations made with other GPCRs[39–41].

To quantitatively examine the extent of the colocalization of two single molecules, we employed a “colocalization index”, which parameterizes the propensity of a pair of magenta and green molecules to become localized within 100 nm. Namely, the colocalization index is defined from the pair cross-correlation function (PCCF) histogram for the SNAP-Surface 549 (green) and SNAP-CF660R (magenta) spots (Fig. 1b)[51], as the ratio of PCCF (0-100 nm) vs. PCCF (400–500 nm) (Supplementary Fig. 2c-e). When a molecular interaction does not exist, the colocalization index is equal to 1 within experimental uncertainty. When it does exist, the index becomes significantly greater than 1. As a negative control (including incidental

Fig. 1 | ORs in the PM form metastable homodimers with lifetimes of 120 ~ 150 ms, without involving the N-terminal extracellular domain. a Typical (among 20 experiments) image sequence of simultaneous two-color single fluorescent molecule observations, showing transient homo-colocalization and co-diffusion of single molecules of SNAPf-KOR tagged with SNAP-CF 660 R (magenta) and SNAP-Surface 549 (green), with their trajectories. **b** PCCFs for the SNAPf-KOR spots (mean ± SEM after area normalization; 18 movies). Green and grey bars indicate the results of the correct and 180°-rotated overlays of the simultaneously observed magenta and green images. The colocalization index is defined as the mean of PCCF values for 0−100 nm divided by the mean of PCCF values for 400−500 nm (see Supplementary Fig. 2c–e). **c** Colocalization indexes showing the homo-colocalizations of three ORs. In the box plots, horizontal bars, crosses, boxes, and whiskers indicate median values, mean values, interquartile ranges (25–75%), and 10–90% ranges, respectively. * and ns represent significant ($p < 0.05$) and non-significant ($p \geq 0.05$) differences, respectively (Tukey's multiple comparison test). The data set used for multiple comparison is indicated by the group of lines in the figure. All of the statistical parameters and analysis results including sample size *n* and *p* values are provided in Supplementary Data 2. **d** Histograms showing the distributions of colocalization durations for correct and rotated overlays. Control histograms for rotated overlays (grey) were fitted by single exponential functions (black), providing the lifetime of the incidental overlap events (τ_{inci}). Histograms for correct overlays (colors) were fitted by the sum of two exponential functions: The faster decay time (τ_1) was close to τ_{inci}, and the slower decay time provided the true homodimer lifetime (τ_2; see Supplementary Note 1 for the theory). The homodimer lifetimes, after correction for the trackable duration lifetimes of the two fluorescent probes, are shown in the boxes. **e** Method to determine the true dissociation rate constant (k_{off}), considering the multiple binding events during an observed colocalization duration. See Supplementary Note 1. Source data are provided as a Source Data file.

colocalization), the 180°-rotated magenta image was superimposed on the green image (see Supplementary Fig. 2d, grey histogram in Fig. 1b), providing a colocalization index of ≈1. KOR, MOR, and DOR exhibited significantly higher colocalization indexes than the negative controls (Fig. 1c), suggesting that they form homodimers (and possibly greater oligomers when the expression levels are enhanced).

Homodimer dissociation rate constant k_{off} (inverse of the dimer lifetime) can be obtained from single-molecule colocalization experiments

To evaluate the homodimer lifetimes, each time we found the colocalization event of spots with different colors within a threshold distance $R = 200$ nm, its duration was measured[40,41,48,49]. By measuring the durations of >1500 events (in ≥17 cells; all statistical parameters are summarized in Supplementary Data 2), we obtained the distribution of colocalization durations (Fig. 1d). In the simultaneous two-color single fluorescent-molecule tracking approach, which is extensively used in this study, we also selected 200 nm as the threshold distance for determining the colocalization of fluorescent spots with two different colors. This is based on, in addition to the consistency with the single-color colocalization threshold distance, the analyses of (1) sensitivity to detect colocalization ("Evaluating colocalization durations" in Methods), (2) avoiding incidental oligomers greater than dimers (Supplementary Fig. 2f; simulation result), and (3) precision of determined homodimer lifetimes (experimental results shown in Supplementary Table 3 related to Supplementary Note 1). Details are provided in "(6) Experimental justification of using a threshold distance *R* of 200 nm" in Supplementary Note 1 and in the subsection "Evaluating colocalization durations" in Methods.

To evaluate the homodimer dissociation rate constant k_{off} (inverse of the homodimer lifetime) from the distribution of colocalized durations, we developed a theory based on the diffusion equation that predicts the distribution of colocalization durations (Supplementary Note 1). The crucial result of this theory is that, from the histogram of the *colocalization* durations, we can rigorously estimate the homodimer dissociation rate constant k_{off} and thus the homodimer lifetime τ_2. Specifically, although the colocalization event of two fluorescent spots is defined by a threshold distance *R*, which is 200 nm in the present study and thus generally much greater than the molecular scale (such as 3–10 nm), we can evaluate the k_{off} and τ_2 values of dimers (associated molecules) by obtaining the duration distribution of the colocalization defined by a threshold distance (such as 200 nm) much greater than the molecular scale. The theory shows that, at a time resolution of 33 ms and under the conditions of quite limited signal-to-noise ratios in our experiments, the histogram of the colocalization durations can be fitted with the sum of two exponential functions, where the two decay constants represent the incidental colocalization lifetime ($1/\alpha$) and the inverse of the dissociation rate constant ($1/k_{\mathrm{off}}$).

Previously, we[40,41,49] and others[28,38,39] depended on intuitive methods to obtain the homodimer lifetimes from optical colocalization data. However, due to the theory developed here, we now have a firm basis to obtain the homodimer dissociation rate constant k_{off} from the distribution of single-molecule colocalization durations.

Brief outline of the theory to evaluate k_{off} from the single-molecule colocalization duration distribution

The full account of this subsection is provided in Supplementary Note 1. In dual-color single-molecule tracking, a colocalization is defined as an event in which two spots are located closer than a threshold distance *R*. Starting from the 2D diffusion equation, we found that the distribution of the dwell times in the threshold circle without binding (incidental lifetime τ_{inci}; i.e., incidental colocalization duration, Fig. 1e) is expressed by

$$p_d(t) \approx \sum_{n=1}^{\infty} \frac{2D\epsilon\mu_n{}^2}{R^3} e^{-\frac{D\mu_n{}^2 t}{R^2}} \approx \alpha e^{-\alpha t} \tag{1}$$

where *D* is the diffusion coefficient, *R* is the threshold distance, ε is a regularization factor, and μ_n is the n-th real positive 0 of the Bessel function (Equation numbers in the main text are not matched with those in Supplementary Note 1 and 2). Under our experimental conditions, the first term is sufficient to describe the distribution, providing a single exponential function with a decay time constant of $R^2/D\mu_1{}^2 = 1/\alpha$, which is the incidental colocalization lifetime (τ_{inci}). We indeed found that the colocalization time distribution for incidental colocalizations obtained for the overlay on the 180°-rotated image (Supplementary Fig. 2d) could be fitted with a single exponential function (using both Akaike's and Bayesian information criteria; AIC and BIC, respectively) (Fig. 1d).

The dwell time in the threshold circle with binding (*T*; i.e., colocalization duration, Fig. 1e) is given by the sum of τ_{inci} added to the sum of multiple binding durations, τ_{i}.

$$T = \tau_{inci} + \sum_{i=1}^{n} \tau_i \tag{2}$$

Here, the terms in the sum correspond to possible multiple binding events during a dwell; i.e., to obtain the correct k_{off} value, we will need to consider the cases where the observed colocalization durations are the results of multiple binding events.

Combining these results, we obtain the dwell time distribution in the threshold circle.

$$P(T) = \frac{\alpha k_{off}}{\Gamma}\left\{\left[1-\frac{(\Delta-\Gamma)}{2k_{off}}\right]e^{-\frac{T}{2}(\Delta-\Gamma)} - \left[1-\frac{(\Delta+\Gamma)}{2k_{off}}\right]e^{-\frac{T}{2}(\Delta+\Gamma)}\right\} \tag{3}$$

where $\Delta = \left(\alpha + k_{\mathrm{off}} + k_{\mathrm{on}}\right)$ and $\Gamma = \sqrt{\Delta^2 - 4\alpha k_{\mathrm{off}}}$.

Table 1 | Summary of K_D (dimer dissociation constant = dimer-monomer equilibrium constant), k_{off} (dimer dissociation rate constant), and k_{on} (dimer formation rate constant) for three ORs without agonists and dimer reference (CD28) and monomer reference (TM^{LDLR}) molecules at 37 °C as well as MOR at 20 °C and FPR(D71A) and D2R dopamine receptor at 37 °C[41]

ORs	K_D (copies/μm^2)	k_{off} (s^{-1})	k_{on} (μm^2/copies/s)
KOR	6.04 ± 0.57	6.71 ± 1.17	1.11 ± 0.22
MOR	15.47 ± 1.54	8.47 ± 0.86	0.55 ± 0.08
DOR	16.62 ± 0.53	8.00 ± 0.96	0.48 ± 0.06
CD28	0.0093 ± 0.03	N.D.	N.D.
TM^{LDLR}	132.00 ± 21.00	N.D.	N.D.
MOR (20 °C)[28]	27.43 ± 11.80	0.56 ± 0.21	0.02 ± 0.004
KOR (20 °C)	5.69 ± 01.11	4.63 ± 0.11	0.81 ± 0.16
KOR (perhaps 20 °C)[35]	32.00 ± 15.00		
FPR(D71A)	2.77 ± 0.55	9.26 ± 0.17	3.61 ± 0.72
FPR(D71A)[41]	3.60 ±0.58	11.0 ± 1.90	3.06 ± 0.72
D2R	33.00 ± 4.61	7.5 ± 0.23	0.23 ± 0.03
D2R[40]		14.6 ± 1.03	

These thermodynamic and kinetic constants have rarely been measured, and all of those we found in the literature[28,35,41] are also listed in this table for comparison.
N.D. for no data.
SEM variations are somewhat large, probably due to limited number of observed movies (approximately 20 movies for 20 cells; the exact numbers are in Supplementary Data 2, along with all other statistical parameters). For comparison with the K_D, k_{off}, and k_{on} values for membrane molecules found in the literature (only four cases were found and shown here), we also performed the measurements for MOR at 20 °C[28], D2R dopamine receptor (D2R)[40], and formyl peptide receptor (FPR(D71A)), at 37 °C[41].

At a time resolution of 33 ms and under the conditions of the quite limited signal-to-noise ratios in our experiments, we obtain

$$(\Delta - \Gamma)/2 \approx k_{\mathrm{off}}, \tag{4}$$

$$(\Delta + \Gamma)/2 \approx \alpha \tag{5}$$

This result explains why the histogram of the colocalization durations can be fitted by the sum of two exponential functions. Most importantly, it permits to identify the two decay constants with the incidental colocalization lifetime (1/α = τ_{inci}) and the inverse of the dissociation rate constant (1/k_{off}), as anticipated.

OR homodimer dissociation rate constant k_{off} and true homodimer lifetime

As shown in Fig. 1d, we were able to fit the three histograms for KOR, MOR, and DOR, obtained from the correctly overlaid images, with the sum of two exponential functions, as predicted by Eqs. 4 and 5. The fitting provided two time constants, τ_1 and τ_2 ($\tau_1 \le \tau_2$). The histogram obtained from the rotated overlay images could be fitted with a single exponential function, which provided the time constant τ_{inci} (= 1/α) (the numbers of significant exponential compontents were always confirmed by both AIC and BIC in this work). We found that $\tau_1 \approx \tau_{\mathrm{inci}}$ for all three ORs. The longer decay time constant obtained from the histogram for the correctly overlaid images (τ_2) provides k_{off} (= 1/τ_2; Supplementary Note 1). As such, using this theory, by simply plotting the histogram of the colocalization durations, we can obtain the correct homodimer dissociation rate constant k_{off} (by taking account of the multiple binding-dissociation cycles).

The homodimer lifetimes of KOR, MOR, and DOR were estimated to be 178 ± 5, 122 ± 3, and 120 ± 3 ms, respectively, from the histograms shown in Fig. 1d (after correction for the trackable duration lifetimes of the two fluorescent probes shown in Supplementary Fig. 2g), providing k_{off} values as summarized in Table 1. We confirmed that the lifetimes of the homodimers were unaffected by the dyes or the tagging proteins at the N- or C-terminus of the ORs (Supplementary Fig. 2h).

To test the theory, we obtained k_{off} values for formyl peptide receptor (FPR(D71A); non-internalization mutant of FPR) and D2R dopamine receptor (both are GPCRs), whose k_{off} values at 37 °C were previously reported[40,41]. The k_{off} values obtained here exhibited reasonable agreement with the previous values (Table 1). Comparisons with the k_{off} values for ORs obtained at 20 °C will be presented in Discussion.

Determination of OR homodimer-monomer equilibrium constant (K_D) from PCCF

In the literature, the question of whether ORs (or GPCRs or any other membrane proteins) form homodimers has been extensively debated. However, it is well estabilished that many membrane proteins would form homodimers and clusters anyway at higher expression levels, and that the OR physiological expression levels would vary greatly from cell to cell in various nerve regions and the local OR number densities in different regions vary greatly within the PM, including the case of MOR assembly in the primary cilia[52]. Therefore, the critical point should be to quantitatively estimate the homodimer affinity; i.e., to evaluate the homodimer dissociation (homodimer-monomer) equilibrium constant K_D. Here, we developed a theory (Supplementary Note 2) for evaluating K_D from the PCCF of the OR fluorescently labeled in two colors (PCCF in the form of a histogram, as shown in Fig. 1b and Supplementary Fig. 2e), under the conditions of low expression levels, where the presence of oligomers greater than dimers could be neglected.

As indicated in Supplementary Note 2, this theory is applicable only to the PCCF data obtained under the conditions of low number densities of membrane molecules (low expression levels) where the occurrences of incidental oligomers greater than dimers are limited (the effect of incidental dimers is included in the theory and so the presence of incidental dimers will not affect the evaluated K_D). Using Monte Carlo simulations, we found that the concentration range employed in this work (1 ± 0.5 copies/μm^2) is quite appropriate to evaluate K_D for values in the range of 1–15 copies/μm^2 (Supplementary Fig. 3a-d). This result was confirmed by experiments using MOR when expression levels were varied in the range of 0.5–1.5 fluorescent spots/μm^2, the actual concentration range employed in this work (Supplementary Fig. 3e; examined by colocalization index).

To estimate the K_D range in which the developed method is applicable, we examined the extreme cases of constitutive monomer and dimer reference molecules: the transmembrane domain of the non-raftophilic monomeric molecule LDL receptor (TM^{LDLR})[41] and the constitutive disulfide-linked dimer molecule CD28[53], respectively. The evaluated K_D values were 132 ± 21 and 0.0093 ± 0.03 copies/μm^2, respectively (Table 1), providing the basic dynamic range (4400x) as well as the limitations of this method to evaluate K_D values.

To further test this method, we evaluated K_D for FPR(D71A) and compared it with the value previously obtained by our more time-intensive method[41]. These K_D values revealed excellent agreement, indicating that our method is reliable (Table 1).

The K_D values obtained for KOR, MOR, and DOR at 37 °C were 6.04 ± 0.57, 15.47 ± 1.54, and 16.62 ± 0.53 copies/μm^2, respectively (Fig. 2a and Table 1; statistical parameters in Supplementary Data 2). These K_D values mean that KOR is more likely to exist as homodimers than MOR and DOR, and thus partially explain previous data showing that KOR, but not DOR or MOR, forms homodimers at low membrane densities[35]. Our estimated values of K_D for the MOR and KOR homodimers exhibited much smaller errors than previous estimates (for

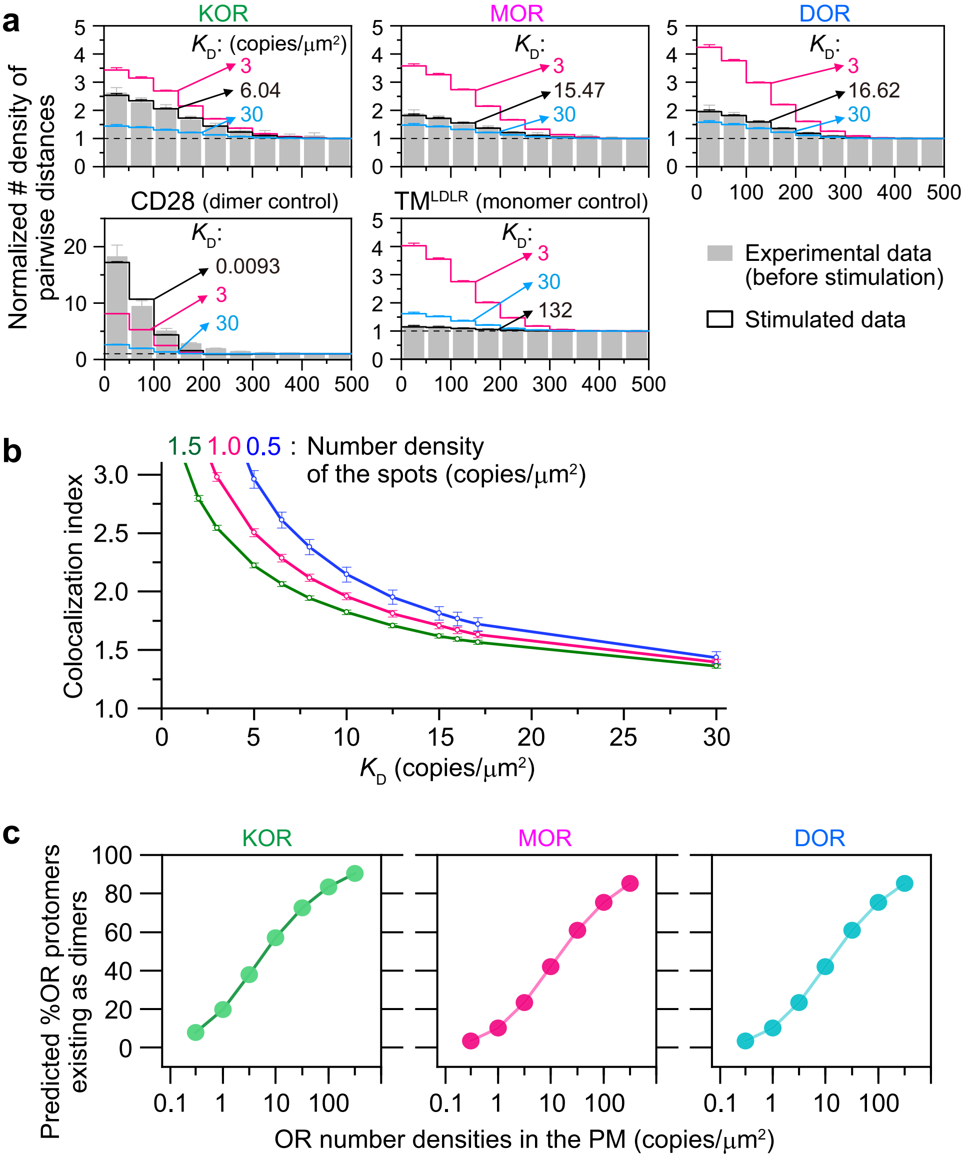

Fig. 2 | Dynamic OR homodimer-monomer equilibrium constants (K_Ds) and homodimer formation and dissociation rate constants (k_{on} and k_{off}, respectively), providing the %protomers existing as dimers as a function of the expression level. a Experimental PCCFs for KOR, MOR, DOR, CD28, and TM^{LDLR} (mean ± SEM, $n = 20$ cells; the PCCF for KOR is the same as that shown in Fig. 1c) and simulated PCCFs for given K_Ds based on the theory described in Supplementary Note 2 (the total numbers of fluorescent spots, sN_{TA} and sN_{TB}, labeling efficiency, and σ were determined from experiments; mean ± SEM, $n = 20$ independent simulations). CD28 and TM^{LDLR} were dimer and monomer references, respectively. The black lines indicate the best-fit functions, and their K_D values are shown. The PCCFs with K_D values of 3 and 30 obtained by simulation (magenta and cyan open bars, respectively) are also shown for comparison. **b** Simulated data showing the relationship between the colocalization index and K_D. Colocalization index decreases monotonically with an increase of K_D, if the labeling efficiency, the precision of single-molecule localization plus image overlaying, and the number density of fluorescent molecules in each movie were the same (0.7, 140 nm, and 0.5, 1, or 1.5 fluorescent spots/μm², respectively). K_D can be roughly estimated from the colocalization index using these curves. (mean ± SEM; $n = 20$ independent simulations) **c** Predicted percentages of OR protomers existing as dimers, plotted as a function of expression levels (without agonist; see Eq. 79 in Supplementary Note 2). The curves indicate the mathematical functions calculated from the K_D values. Tick marks between the exact digits represent ≈3.16x ($10^{0.5}$x) of the smaller digit. In this study, since labeling efficiencies were 66% and 61% for SNAP-Surface 549 and SNAP-CF660, respectively, and the dimer spots generally represents only 5–10% of the spots (because 10-20% of ORs exist as homodimers), the OR expression levels in the observed cells are expected to be approximately 1.8 molecules/μm². OR expression levels would greatly vary depending on particular PM domains, nerve circuits, and various pathological and pharmacological conditions[26–32]. Source data are provided as a Source Data file.

MOR[28], 27.43 ± 11.75 copies/μm²; and for KOR[35], 32 ± 15 copies/μm²), and their mean values are smaller by factors of approximately 1.7 and 4.9, respectively. The reason for these differences is unknown, but note that our SEMs relative to the means are much smaller than previous estimates of the K_D values.

In the following part of this report and in the companion paper[42], we use the colocalization index when showing the direct experimental data is preferable, whereas the K_D values are presented when providing the fundamental constants is desirable. Under our standard experimental conditions, the colocalization index is simply related to K_D as shown in Fig. 2b (justifying the use of the colocalization index in Supplementary Fig. 3e), and K_D can be roughly evaluated using the graphs shown there, although we performed actual fitting for the PCCF for each cell to obtain the K_D value for each cell (the final K_D value and its SEM were obtained as the arithmetic mean of the K_Ds for all the observed cells).

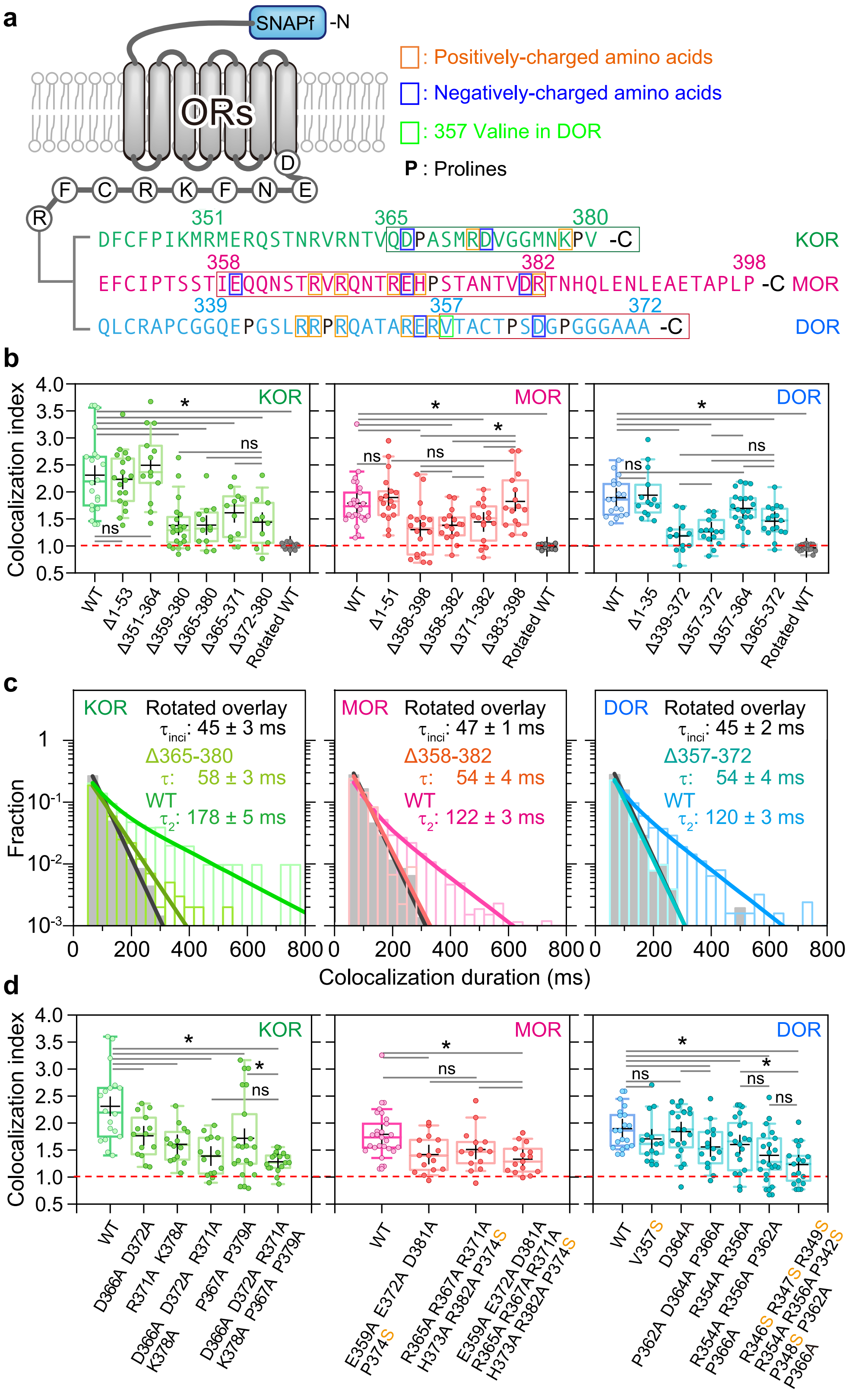

Using k_{off} and K_D, k_{on} can be calculated as k_{off}/K_D (Eq. 1 in Supplementary Note 2). Direct determination of k_{on} from single-molecule movies is only possible when the labeling efficiency is 100%. This is because the fluorescent spots that appear to be monomers (protomers) of A and B molecules might be dimers of labeled and non-labeled molecules (Supplementary Table 4 related to Supplementary Note 2). For the correction to evaluate the actual numbers of protomers, one would need to know K_D, and thus k_{on} cannot be determined independently from K_D. The percentages (in copy numbers) of molecules (protomers) that exist as dimers at various expression levels (number density of molecules) were calculated from the obtained K_D values (Fig. 2c). Their overall variations are in the range of 3.4–58% of protomers in homodimers at number densities of 0.3–10 copies/μm^2, the experimental expression range often employed[26–28].

Fig. 3 | C-terminal cytoplasmic domains are predominantly responsible for OR homodimerization. a Schematic figure showing the amino-acid sequences of the C-terminal cytoplasmic domains of the three ORs. The sequences surrounded by rectangles were extensively examined for their involvement in OR homodimerization. **b** Colocalization indexes for WT and various N/C-terminal deletion mutants, showing that KOR aa 365-380, MOR aa 358-382, and DOR aa 357-372, with very low amino-acid homologies, are critical for homodimerization. **c** Histograms showing the distributions of colocalization durations for the C-terminal cytoplasmic deletion mutants, KOR(Δ365-380), MOR(Δ358-382), and DOR(Δ357-372) (only the results of correct overlays). WT-OR data are reproduced for comparison (for both correct and rotated overlays; Fig. 1d). Deletion mutants exhibited distributions that could be fitted by single exponential functions, and their decay time constants τs (after correction for the trackable duration lifetimes of the two fluorescent probes) are indicated in the boxes. **d** The colocalization indexes of various C-terminal point mutants, indicating that the charged groups and prolines in the C-terminal cytoplasmic domains play important roles in OR homodimerization. In the box plots (**b, d**), horizontal bars, crosses, boxes, and whiskers indicate median values, mean values, interquartile ranges (25–75%), and 10-90% ranges, respectively. * and ns represent significant ($p < 0.05$) and non-significant ($p \geq 0.05$) differences, respectively (Tukey's multiple comparison test). The data set used for multiple comparison is indicated by the group of lines in each figure. All of the statistical parameters and analysis results including sample size *n* and *p* values are provided in Supplementary Data 2. Source data are provided as a Source Data file.

Therefore, substantial amounts of homodimers would exist in various nerve tissues at any time. The expected average protomer copy numbers existing as monomers and homodimers per cell at various expression levels are calculated and shown in Fig. 2c and Table 1. However, all of these homodimers are forming and dispersing all the time, with lifetimes shorter than 0.2 s (Fig. 1d). Once dissociated into monomers, they will again form homodimers, often with different partner molecules (Supplementary Fig. 2a, b), which will occur more readily at higher expression levels. Therefore, although at any moment, 10–20% of ORs might exist as homodimers at the expression levels we employed (≈1 spot/μm^2) (Fig. 2c), the actual molecules existing as dimers are turning over all the time, and within a few seconds (even at an expression level of 1 copy/μm^2; calculated as $1/k_{off} + 1/[k_{on} \text{ x } 1]$), virtually all of the molecules experience the periods of homodimers and monomers. In addition, from these values, our experimental condition of ≈1 fluorescent spot/μm^2 can be converted to molecular expression levels of ≈1.8 OR molecular copies/μm^2 (caption to Fig. 2c).

The 9-26 amino-acid sequences in the C-terminal cytoplasmic domains play critical roles in OR homodimerization

To advance our understanding of OR homodimerization mechanism, we determined the OR domains and amino acid sequences responsible for homodimerization (Fig. 3a; Supplementary Fig. 4a). First, we examined the involvement of the extracellular N-terminal domains in homodimerization, using the N-terminal deletion mutants (KOR(Δ1-53), MOR(Δ1-51), and DOR(Δ1-35)) (Fig. 3b). Given that the amino-acid homologies in the N-terminal domains among the three ORs are quite low, we considered a possibility that they might be used to distinguish particular homo- and hetero-dimers. These amino-acid sequence ranges were selected partly because the removal of the entire N-terminal extracellular domains blocked the OR expression in the PM, probably due to the deletion of the signal sequences. In addition, these deletion mutants were previously used in X-ray crystallography studies to determine the structures of the remaining parts of ORs[54–57].

The N-terminal deletion mutants of the three ORs all exhibited diffusion behavior similar to those of the wild types (without immobilization or clustering) and virtually the same colocalization indexes as those of the wild types (Fig. 1c). These results clearly indicate that the N-terminal extracellular domains are not responsible for homodimerization.

We next examined the involvement of the C-terminal cytoplasmic domains. Their amino-acid homologies are also low, and in addition, a previous biochemical analysis indicated that the 15-amino acid stretch in the C-terminal domain is responsible for DOR homodimerization[9]. We examined systematically varied C-terminal deletion mutants (Fig. 3a, b). They hardly exhibited immobility or clustering, and their colocalization indexes showed that KOR's aa 365-380, MOR's aa 358-382, and DOR's aa 357-372 are critical for homodimerization (Fig. 3b and Supplementary Data 2). For DOR, this amino-acid sequence agrees with the previous biochemical data[9]. Meanwhile, the mean colocalization index values never decreased to the index values comparable to those for rotated overlays (≈1) (Fig. 3b) or a monomer control molecule TM^{LDLR} (≈1.1) (Fig. 2a), suggesting the possible presence of other weaker homodimerization site(s), which we will discuss later.

The distribution (histogram) of the colocalization durations for each representative deletion mutant, KOR(Δ365-380), MOR(Δ358-382), or DOR(Δ357-372), could be fitted by a single exponential function (τ), rather than the sum of two exponential functions (based on both AIC and BIC). The decay time constants (τ's) were slightly longer than the incidental colocalization lifetimes (τ_{inci}, Fig. 3c). We speculate that these slightly longer decay time constants for these deletion mutants (τ's) compared to τ_{inci}'s are due to the existence of weak homodimerizations whose lifetimes are quite close to τ_{inci}'s and/or to the presence of very small fractions of homodimers. The lifetimes of such components could not be separated from the τ_{inci} component, but they would make the decay time constants (τ's) longer than τ_{inci}'s.

By introducing point mutations in these critical regions for homodimerization and their surrounding regions (Fig. 3a), we found that a few to several basic/acidic residues, as well as proline residues, are involved in the OR homodimerization (for particular amino acids, see the colocalization indexes shown in Fig. 3d), suggesting that the electrostatic interactions and the overall structure of the cytoplasmic C-terminal domain could be important for homodimerization. The importance of electrostatic interactions in the cytoplasmic domains of GPCRs has been previously stressed[58]. For the overall structure of the cytoplasmic C-terminal domain, the IUPred2 scores (energy-estimation-based predictions for ordered and disordered residues; http://iupred2a.elte.hu)[59,60] indicated that the C-terminal region could be weakly intrinsically disordered (Supplementary Fig. 4b), and the scores decreased (more ordered) with the point mutations examined here (Supplementary Fig. 4c). Accordingly, in addition to the specific, relatively strong amino-acid interactions, multiple specific but weak interactions, made possible by the flexible intrinsically disordered regions (IDRs) of the ORs' C-terminal regions, might facilitate the OR homodimerization. Such a mechanism resembling liquid-liquid phase separation was previously found for the dimerization of the transcription factor PU.1[61]. Furthermore, the IDRs in the C-terminal regions might be necessary to bring the specific binding sites closer so that the actual binding can occur[62]. AI-based structure prediction of the homodimers of ORs' C-terminal cytoplasmic domains could only be performed for DOR using Chai Discovery software, and its highest-ranking average structure exhibited 180° rotational symmetry (Supplementary Fig. 5), although the IDRs are likely to undergo rapid and large conformational fluctuations.

Peptides mimicking the homodimerization sites block homodimer formation

We then examined whether peptides with the same amino-acid sequences as those of the deleted parts of the mutants could block homodimerization. The use of these peptides was critical for

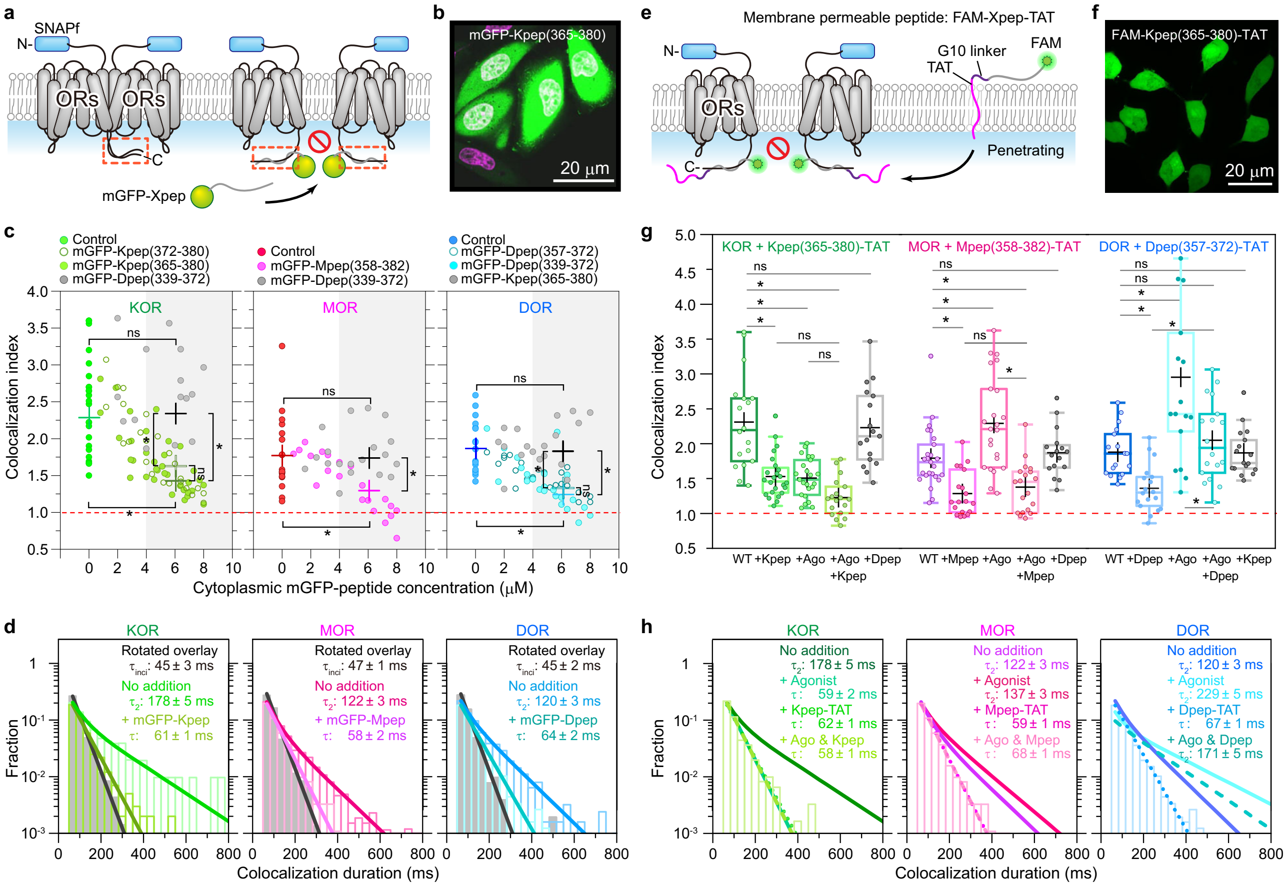

Fig. 4 | Specific C-terminal-domain peptides suppress OR homodimerization. **a** Schematic figure showing the experimental design to examine the effects of mGFP-Xpeps expressed in the cell on OR homodimerization. **b** Representative (among 20 replicates) confocal image of CHO-K1 cells transfected with cDNAs encoding SNAPf-KOR (not visible here; only visible by single-molecule imaging conditions) and mGFP-Kpep (green), co-stained with the Live 650 Nuclear Stain (magenta; white nuclei indicate the entrance of mGFP-Kpep into the nuclei, whereas a magenta nucleus indicates the cell without mGFP-Kpep expression). **c** The OR homo-colocalization index in each cell tends to decrease with an increase of the mGFP-Xpep concentration in the cytoplasm. The + keys at x = 0 and 6 μM mGFP-Xpep indicate the mean value of the colocalization indexes without mGFP-Xpep expression and that averaged over all the data points in the range of 3.8–7.8 μM mGFP-Xpep, respectively. **d** Histograms showing the duration distributions of transient homodimers of SNAPf-ORs in cells co-expressing 3.8–7.8 μM mGFP-Xpeps, compared with those without co-expression (for both correct and rotated overlays). **e** Schematic figure showing the experimental design to examine the effect of the FAM-Xpep-TATs incorporated in the cell on OR homodimerization. **f** Representative confocal image of CHO-K1 cells containing an average of 3.4 μM FAM-Kpep-TAT in the cytoplasm. Representative of three independent experiments with similar results. **g, h** Agonist addition (0.2 μM) suppressed KOR homodimerization, but enhanced the homodimerization of MOR and DOR (colocalization indexes in **g** and durations of colocalization events in **h**). The presence of ≈3 μM FAM-Xpep-TAT in the cytoplasm suppressed homodimerization both before and 2–5 min after the agonist addition. In the box plots, horizontal bars, crosses, boxes, and whiskers indicate median values, mean values, interquartile ranges (25–75%), and 10–90% ranges, respectively. * and ns represent significant ($p < 0.05$) and non-significant ($p \geq 0.05$) differences, respectively (Tukey's multiple comparison test). All of the statistical parameters and analysis results including sample size *n* and *p* values are provided in Supplementary Data 2. Source data are provided as a Source Data file.

unequivocally demonstrating that the specific amino-acid sequences in the C-terminal regions of KOR, MOR, and DOR are responsible for homodimerizations, because the deletion and point mutations might have induced conformational changes of the true homodimer interaction sites, thus inhibiting homodimerization. Furthermore, if we could develop such homodimerization blockers, they could become useful tools to dissect the functions of OR monomers and homodimers, and might inform future developments of more effective analgesic treatments with fewer side effects and less tolerance development[2,9,11–13,20,63].

We employed two approaches. The first one involved the expression of peptides with the same amino-acid sequences as those of the deleted parts of the mutants (named Kpep, Mpep, and Dpep), conjugated to the C-terminus of mGFP (named mGFP-Kpep, -Mpep, and -Dpep, respectively, collectively called mGFP-Xpeps; numbers in parentheses following mGFP-Xpeps indicate the amino-acid residue ranges in the wild-type ORs) (Fig. 4a) in CHO-K1 cells stably expressing SNAPf-KOR, -MOR, or -DOR, respectively. The concentration of the cytoplasmic mGFP-Xpep was measured by confocal fluorescence microscopy (representative image shown in Fig. 4b), based on calibration with various concentrations of purified mGFP protein dissolved in Ham's F12 observation medium in the glass-base dish (Supplementary Fig. 6a; see Methods).

The OR homo-colocalization index in the cells expressing various concentrations of mGFP-Xpep in the cytoplasm (homogeneously distributed throughout the cytoplasm; Fig. 4b) exhibited a clear tendency to decrease with an increase of the specific mGFP-Xpep concentration in the cytoplasm from 0 to 7.8 μM for all three ORs, whereas the control mGFP-peptides (mGFP-Dpep for KOR and MOR and mGFP-Kpep for DOR) had no effect (Fig. 4c). Consistently, the distributions of the colocalization durations in cells expressing 3.8–7.8 μM mGFP-Xpeps could be fitted by a single exponential function, rather than the sum of

https://doi.org/10.1038/s41467-025-64694-3

Table 2 | Summary of the colocalization indexes, homodimer lifetimes, fractions and PM residency times of molecules with internalizations detectable by the 35 min observations, and Ca^{2+} mobilization parameter, $(F_{Max}\text{-}F_b)/F_b$, in the presence and absence of various modulators (0.2 μM agonists, ≈ 3 μM FAM-Xpep-TATs in the cytoplasm, and ≈ 6 μM mGFP-Xpeps in the cytoplasm)

ORs	Additions	Colocalization Index (Mean ± SEM)	Homodimer Lifetime (ms) (Mean ± SEM)	Fraction of internalized molecules (%)	PM residency time of internalized molecules (min)	Ca^{2+} $(F_{Max}\text{-}F_b)/F_b$
KOR	Control	2.30 ± 0.2	178 ± 5	8.4 ± 4.1	32.1 ± 23.8	0.04 ± 0.01
	+ FAM-pep-TAT	$1.53 \pm 0.1^{a,Na}$	$62 \pm 1^{a,Na}$	$6.9 \pm 2.4^{Nc,b}$	$26.2 \pm 15.4^{Nc,b}$	$0.05 \pm 0.01^{Nc,b}$
	+ mGFP-pep	$1.41 \pm 0.1^{a,Na}$	$61 \pm 1^{a,Na}$	-	-	-
	+ Agonist	1.48 ± 0.1^{a}	59 ± 2^{a}	51.4 ± 2.7^{a}	11.9 ± 1.7^{a}	1.96 ± 0.32^{a}
	+ Agonist + FAM-pep-TAT	$1.23 \pm 0.1^{a,b}$	$58 \pm 1^{a,Na}$	$60.5 \pm 2.5^{a,b}$	$9.6 \pm 1.2^{a,Na}$	$2.46 \pm 0.21^{a,b}$
	+ Agonist + mGFP-pep	$1.17 \pm 0.1^{a,b}$	$54 \pm 2^{a,Na}$	-	-	$3.11 \pm 0.17^{a,b}$
MOR	Control	1.82 ± 0.1	122 ± 3	6.4 ± 1.9	25.8 ± 12.6	0.03 ± 0.01
	+ FAM-pep-TAT	$1.38 \pm 0.1^{a,b}$	$59 \pm 1^{a,b}$	$6.3 \pm 1.0^{Nc,b}$	$22.1 \pm 4.1^{Nc,b}$	$0.04 \pm 0.01^{Nc,b}$
	+ mGFP-pep	$1.32 \pm 0.1^{a,b}$	$58 \pm 2^{a,b}$	-	-	-
	+ Agonist	2.18 ± 0.2^{a}	137 ± 3^{a}	28.1 ± 1.7^{a}	11.3 ± 1.9^{a}	2.80 ± 0.21^{a}
	+ Agonist + FAM-pep-TAT	$1.38 \pm 0.1^{a,b}$	$68 \pm 1^{a,b}$	$28.9 \pm 2.0^{a,Na}$	$10.7 \pm 2.1^{a,Na}$	$2.78 \pm 0.22^{a,Na}$
	+ Agonist + mGFP-pep	$1.34 \pm 0.1^{a,b}$	$67 \pm 3^{a,b}$	-	-	$2.80 \pm 0.24^{a,Na}$
DOR	Control	1.89 ± 0.1	120 ± 3	4.5 ± 3.5	29.8 ± 37.4	0.05 ± 0.01
	+ FAM-pep-TAT	$1.36 \pm 0.1^{a,b}$	$67 \pm 1^{a,b}$	$4.9 \pm 2.5^{Nc,b}$	$26.2 \pm 22.6^{Nc,b}$	$0.05 \pm 0.01^{Nc,b}$
	+ mGFP-pep	$1.29 \pm 0.1^{a,b}$	$64 \pm 2^{a,b}$	-	-	-
	+ Agonist	3.00 ± 0.3^{a}	229 ± 5^{a}	61.6 ± 1.7^{a}	10.8 ± 0.9^{a}	3.85 ± 0.23^{a}
	+ Agonist + FAM-pep-TAT	$2.08 \pm 0.2^{a,b}$	$171 \pm 5^{a,b}$	$55.0 \pm 1.0^{a,b}$	$10.1 \pm 0.5^{a,Na}$	$2.84 \pm 0.20^{a,b}$
	+ Agonist + mGFP-pep	$2.00 \pm 0.2^{a,b}$	$168 \pm 5^{Nc,b}$	-	-	$2.65 \pm 0.22^{a,b}$

The agonists employed here were U-50488 for KOR, DAMGO for MOR, and SNC-80 for DOR.

$^{a\,(Nc)}$: Significant (insignificant) difference from the value for "Control".

$^{b\,(Na)}$: Significant (insignificant) difference from the value for "+ Agonist".

Significant and insignificant differences were determined by $p < 0.05$ and $p \geq 0.05$, respectively. *P* values and statistical parameters for all results throughout this report are included in Supplementary Data 2. The *p* values were obtained by Tukey's multiple comparison test, except the Brunner-Munzel test used for colocalization lifetimes. All data shown in this paper are the results of at least three independent replicates.

two exponential functions (based on both AIC and BIC; Fig. 4d), and the decay time constants became similar to those for the C-terminal deletion mutants (compare Fig. 4d with Fig. 3c; Table 2).

As the second approach, Kpep, Mpep, and Dpep were conjugated with the fluorescent dye 5-FAM at their N-termini for visualization, and with the TAT sequence (YGRKKRRQRRR) (using a G10 linker sequence) at their C-termini for membrane permeabilization (FAM-Xpep-TAT). These FAM-Xpep-TATs were added to the cells preincubated with 150 μM pyrenebutyrate for 5 min to enhance the efficiency of peptide translocation across the membrane (Fig. 4e, f; see Methods)[64]. The FAM-peptide-TATs exhibited diffuse spatial distributions throughout the cytosol (Fig. 4f). The cells containing 2.9–3.4 μM FAM-Xpep-TAT (see Supplementary Fig. 6b for the concentration calibration; in the following, we describe this concentration range as ≈3 μM for conciseness) were selected and the effects of these cytoplasmic peptides on the OR homodimerization were examined. The results indicated that ≈3 μM FAM-peptide-TAT significantly blocked the homo-dimerization (Fig. 4g; Table 2), consistent with the data obtained using mGFP-Xpeps (Fig. 4c). The efficiency of blocking homodimerization by FAM-Xpep-TAT is greater than that by mGFP-Xpep (at ≈3 μM), probably due to the steric hindrance of mGFP (Fig. 4c, g). The control FAM-Xpep-TATs (FAM-Dpep-TAT for KOR and MOR and FAM-Kpep-TAT for DOR) did not affect the colocalization indexes. The effects on colocalization durations (Fig. 4h) were consistent with the colocalization index data and with those obtained by expressing mGFP-Xpeps (Fig. 4h; compare with Fig. 4d; Table 2).

The Xpep concentrations required for blocking homodimer formation might appear quite high (≈ 3 μM), compared with the ≈30-nM-level dissociation constants of various agonists and antagonists for ORs. However, note that the latter is the value for simple binding of the ligand to the receptor, whereas the former addresses the efficient dimerization propensities of membrane molecules in the two-dimensional (2D) PM. The efficiency of dimerization in 2D space was previously found to be higher by a factor of 10^6 than that in 3D space[65].

The effects of the presence of ≈3 μM FAM-Xpep-TATs in the cytoplasm on the homodimer K_D, k_{off}, and k_{on} values are summarized in Table 3. In addition to K_D and k_{on}, FAM-Xpep-TATs increased k_{off} (enhanced dimer dissociation), indicating that the OR homodimerization cannot be described by simple first-order kinetics (simple binding reaction at the C-terminal domains), perhaps due to the conformational changes of the C-terminal domains induced by the peptide binding and/or to the presence of weaker secondary binding sites,

Table 3 | Summary of K_D, k_{off}, and k_{on} for three ORs in the presence and absence of ≈ 3 μM FAM-Xpep-TAT in the cytoplasm, both before and 2–5 min after the addition of agonists

ORs	Agonist	Xpep	K_D (copies/μm^2)	k_{off} (s^{-1})	k_{on} (μm^2/copies/s)	Predicted %OR protomers existing as dimers at five expression levels: 0.3, 1, 3, 10, and 30 (copies/μm^2)				
						0.3	1	3	10	30
KOR	–	–	6.04 ± 0.57	6.71 ± 1.17	1.11 ± 0.22	8.3	20	38	58	73
	–	+	58.45 ± 6.73	16.13 ± 0.26	0.28 ± 0.03	1.0	3.2	8.6	21	39
	+	–	16.01 ± 1.36	17.86 ± 0.32	1.12 ± 0.10	3.5	10	23	42	60
	+	+	65.47 ± 16.0	17.24 ± 0.30	0.26 ± 0.06	0.9	2.9	7.8	20	37
MOR	–	–	15.47 ± 1.54	8.47 ± 0.86	0.55 ± 0.08	3.6	10	23	43	61
	–	+	46.06 ± 7.99	16.95 ± 0.29	0.37 ± 0.06	1.3	4.0	10	25	43
	+	–	8.54 ± 0.58	5.35 ± 1.69	0.63 ± 0.20	6.2	16	32	53	69
	+	+	57.00 ± 8.20	14.71 ± 0.22	0.26 ± 0.04	1.0	3.3	8.8	22	39
DOR	–	–	16.62 ± 0.53	8.00 ± 0.96	0.48 ± 0.06	3.4	9.8	22	41	59
	–	+	41.72 ± 3.29	14.93 ± 0.22	0.36 ± 0.03	1.4	4.4	11	26	44
	+	–	7.89 ± 0.36	3.62 ± 0.25	0.46 ± 0.04	6.6	17	34	54	70
	+	+	19.90 ± 1.82	5.88 ± 0.17	0.30 ± 0.03	2.8	8.4	20	38	57

Predicted percentages of OR protomers existing as dimers at various expression levels calculated from the K_Ds are also shown.

which will be discussed later. Nevertheless, we consider the present simplified approach is useful as the starting point for quantitative understanding of the dynamic equilibrium between OR homodimers and monomers.

Agonists modulate monomer-dimer interconversions, and FAM-Xpep-TAT peptides reduce their effects

The addition of representative agonists, U-50488 for KOR, [D-Ala^2, N-Me-Phe^4, Gly^5-ol]-enkephalin acetate salt (DAMGO) for MOR, and SNC-80 for DOR, at 0.2 μM (a concentration sufficient to ligate virtually all OR molecules) differently affected the homodimerization of the three ORs (observed during 2–5 min after agonist addition rather than after longer incubation, because these agonists induce OR internalizations, which become evident after 5 min; discussed later in this report). The agonist-bound KOR exhibited less homodimerization (lower colocalization index), whereas the agonist-bound MOR and DOR exhibited more homodimerization (Fig. 4g and Table 2), although these results might vary depending on the particular agonist[9,14]. The colocalization indexes of the agonist-bound ORs were reduced by the addition of FAM-Xpep-TAT for all ORs, but in different ways depending on the OR type (Fig. 4g). The colocalization index of the agonist-bound KOR, which exhibited a smaller index as compared with that of non-ligated KOR, was further reduced by the presence of FAM-Kpep-TAT (although with no statistical significance). The colocalization index of the agonist-bound MOR was reduced in the presence of FAM-Mpep-TAT to a level near that for MOR with the FAM-Mpep-TAT without the agonist. The colocalization index of the agonist-bound DOR was reduced in the presence of FAM-Dpep-TAT, but was still greater than that of wild-type DOR in the absence of the agonist, which will be described in the next subsection. The effects of the agonists and homodimer blocker peptides on the colocalization durations were consistent with the colocalization index data (Fig. 4h), and the agonists' effects on the homodimer K_D, k_{off}, and k_{on}, as well as the percentages of OR protomers existing as homodimers are summarized in Table 3. The actual copy numbers of OR protomers existing as monomers and homodimers at various total numbers of OR molecules in the entire PM in a cell are summarized in Supplementary Table 1.

MOR's transmembrane domain 1 (TM1^{MOR}) is involved in MOR homodimerization with less specificity

Specific C-terminal cytoplasmic domain deletions/mutations and the addition of peptides with the same amino acid sequences as the deleted sequences greatly reduced the OR homodimers' colocalization indexes, but never to be compatible with 1 found for rotated overlays or 1.1 found for the monomer control molecule TM^{LDLR} (Fig. 2a). Therefore, we considered the existence of secondary sites for homodimer formation. Since the involvement of transmembrane domains in the homo- and hetero-dimerization of ORs[20,26,33,55,56,66,67] and in homodimerization of other class A GPCRs[21,43–45,68] has been proposed, and the first OR transmembrane domain (TM1) is often mentioned in the literature[26,55,56], we examined the involvement of MOR's TM1 domain (TM1^{MOR}) in MOR homodimerization (Fig. 5a).

Colocalization indexes indicated that TM1^{MOR} interacts with another TM1^{MOR} and MOR, as well as, importantly, with DOR (Fig. 5b; the fluorescent spot number densities of the two molecules in the PM were always adjusted to ≈1 spot/μm^2, and thus the number ratio was approximately 1:1). The control TM peptide (TM^{LDLR}) showed no interaction with either receptor.

These results suggest that TM1^{MOR} is involved in MOR homodimerization by the TM1^{MOR}-TM1^{MOR} interaction, as well as, surprisingly, in MOR-DOR heterodimerization. These results are supported by the observation of the colocalization durations (Fig. 5c).

In contrast, in the homodimer blocking experiments where TM1^{MOR} is expressed ≈10-fold more than MOR, DOR, or KOR (Fig. 5d, e), TM1^{MOR} moderately suppressed both MOR and DOR homodimers, but not KOR homodimers (compare with the results after the addition of positive control molecules, Mpep, Dpep, or Kpep, respectively, and the results observed in the presence of negative control molecules, TM^{LDLR} and Xpeps specific for different OR homodimers) (Fig. 5e). More specifically, while TM1^{MOR} reduced both MOR and DOR homodimers, Mpep selectively reduced MOR homodimers without affecting DOR homodimers, and Dpep selectively reduced DOR homodimers without affecting MOR or KOR homodimers. The absence of a TM1^{MOR} effect on KOR homodimerization is consistent with the lack of MOR-KOR heterodimerization[42]. Taken together, we conclude that the interaction specificity of TM1^{MOR} is limited as shown from its ability to interact with both MOR and DOR (Fig. 5b, e). The results showing that TM1^{MOR} suppresses both MOR-MOR and DOR-DOR homodimerization indicate that TM1^{MOR} is involved in both MOR homodimerization and MOR-DOR heterodimerization. These results further indicate that TM1^{MOR} might not be useful as a specific blocker for MOR homodimerization or MOR-DOR heterodimerization.

Cholesterol and the lipid microenvironment might affect OR homodimerization[21,69]. Cholesterol depletion and cholesterol repletion

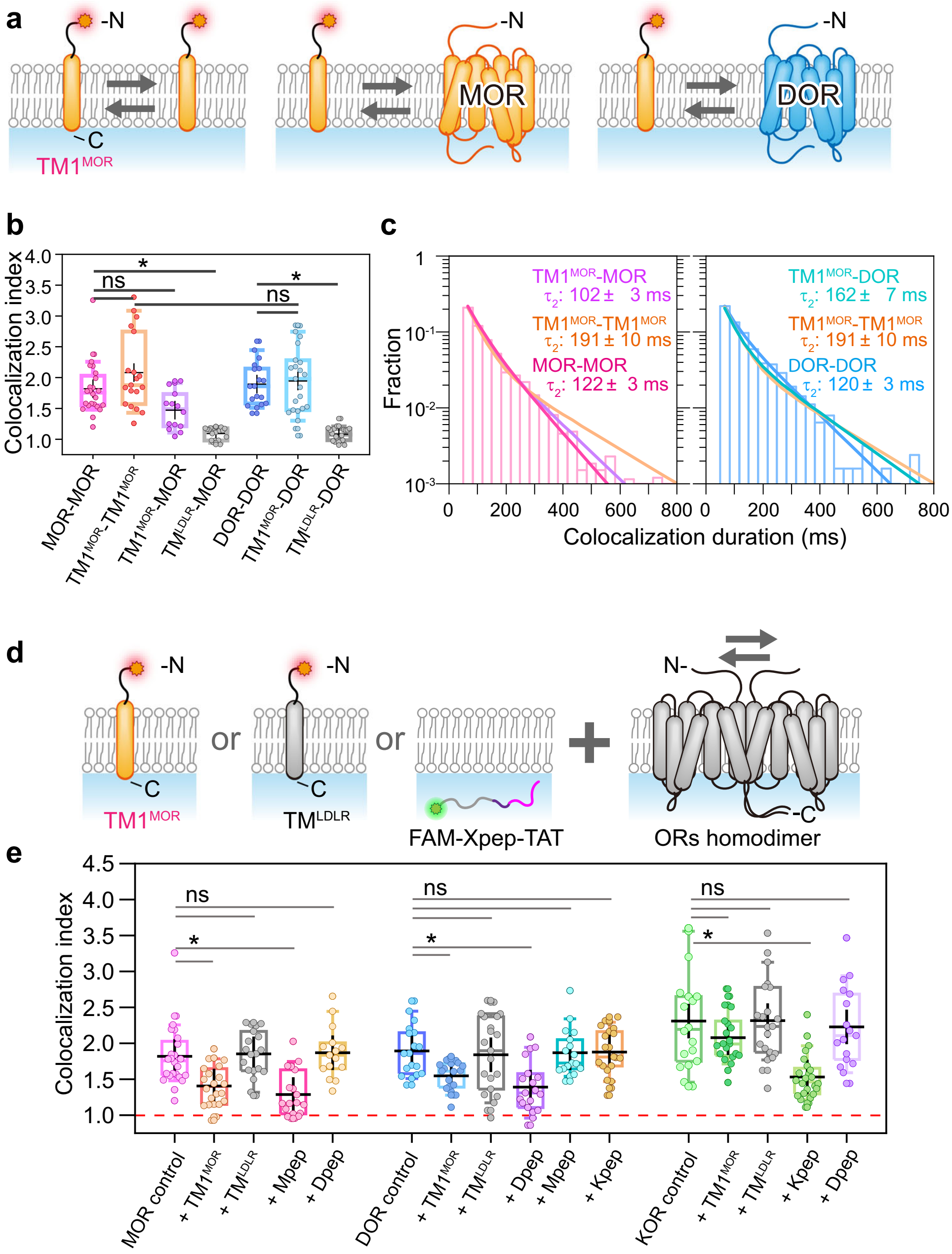

Fig. 5 | TM1^{MOR} suppresses both MOR and DOR homodimerization. a Schematic figure showing the experimental design for examining the interaction (binding) of TM1^{MOR} with itself, MOR, and DOR. Colocalization indexes (**b**) and distributions of colocalization durations (**c**) showing that TM1^{MOR} forms metastable dimers with both MOR and DOR, while the control TM peptide (TM^{LDLR}) shows no interaction with either receptor, suggesting that TM1^{MOR} might be involved in MOR-MOR homodimerization as well as MOR-DOR heterodimerization[42]. **d** Schematic figure showing the experimental design for examining whether TM1^{MOR} can suppress homodimerizations of MOR and DOR. **e** TM1^{MOR} suppresses homodimerization of both MOR and DOR, but not KOR. In contrast, Mpep, Dpep, and Kpep selectively inhibit the homodimerization of MOR, DOR, and KOR, respectively. TM^{LDLR} hardly affects any OR homodimerization. In the box plots (**b, e**), horizontal bars, crosses, boxes, and whiskers indicate median values, mean values, interquartile ranges (25–75%), and 10-90% ranges, respectively. * and ns represent significant ($p < 0.05$) and non-significant ($p \geq 0.05$) differences, respectively (Tukey's multiple comparison test). All of the statistical parameters and analysis results including sample size *n* and *p* values are provided in Supplementary Data 2. Source data are provided as a Source Data file.

followed by depletion did not affect the MOR homodimer lifetime. The MOR homodimer lifetime remained virtually the same in GM3-null cells (produced from the CHO-K1 cells, which are used in other experiments in this investigation; Supplementary Fig. 7)[70].

No major effects of Xpeps on the agonist-induced OR internalization

We next examined whether OR monomers and homodimers are engaged in different signaling functions and internalization behaviors before and after the agonist addition. The relative amounts of ORs undergoing Gi-coupled signaling vs. those becoming internalized would be related to OR's biased signaling, which is pharmacologically crucial as they are linked to opioid efficacy vs. side effects and tolerance development. The biased responses upon agonist addition might be quite different between OR monomers and dimers, and therefore, we examined the agonist-induced signaling and internalization of OR monomers and homodimers.

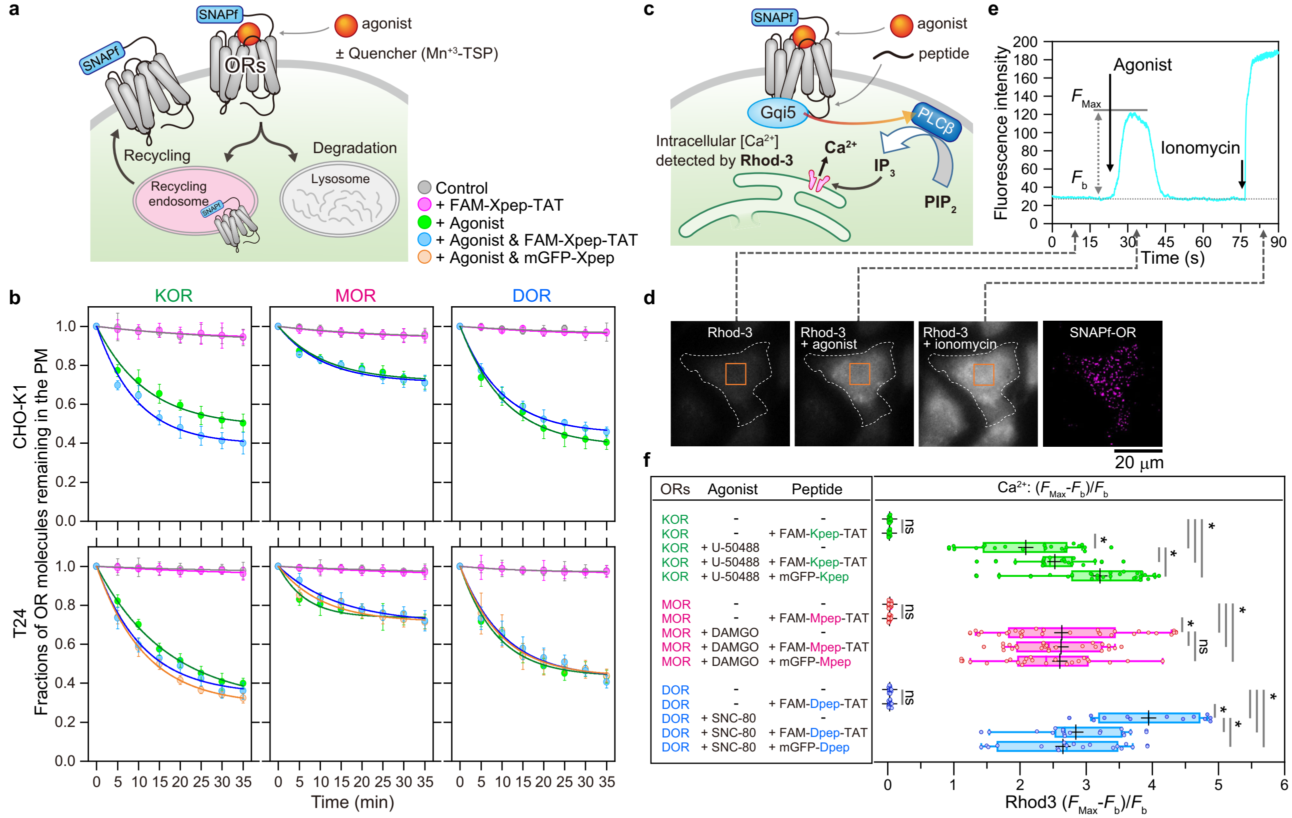

Fig. 6 | Xpeps hardly affect OR internalization in both the presence and absence of the agonist, whereas they enhanced, did not affect, or reduced the Ca^{2+} mobilization induced by the KOR, MOR, and DOR agonists, respectively. **a** Schematic figure showing the experimental design for observing the internalization of OR (with possible recycling). Also see Supplementary Fig. 8a. **b** Time-dependent decreases of SNAPf-ORs on the PM due to their internalizations in CHO-K1 cells (top) and T24 cells (bottom) (mean ± SEM; 10 cells for each data point), before and after the addition of 0.2 μM agonist in the presence and absence of ≈3 μM FAM-Xpep-TATs and ≈6 μM mGFP-Xpeps in the cytoplasm. Photobleaching of the fluorescent probe is negligible because only one frame was recorded every 5 min. The time courses could be operationally fitted by single exponential functions, $y = C\cdot\exp(-t/\tau_0) + (1-C)$, providing the fractions of OR molecules with detectable (C) and non-detectable (1 - C) internalizations for the observations up to 35 min, as well as the residency times (τ_0) for the internalized component. **c** Schematic figure showing the experimental design for observing the Ca^{2+} mobilization after the agonist stimulation. The Ca^{2+} mobilization was monitored by the Rhod-3 fluorescence intensity (see Methods). **d, e** Typical (among 20 cells) fluorescence images of Rhod-3 in cells (**d**; orange rectangles = ROI) and the time-dependent changes of the Rhod-3 signal intensity in the ROI (**e**), showing the changes in the cytosolic Ca^{2+} concentration after the agonist stimulation. Cells with similar expression levels of ORs (≈1 fluorescent spot/μm^2) were selected. **f** Ca^{2+} mobilization at 75 s after the agonist addition, parametrized by using $[F_{Max}-F_b]/F_b$ (see **e**). In the box plots, horizontal bars, crosses, boxes, and whiskers indicate median values, mean values, interquartile ranges (25–75%), and 10–90% ranges, respectively. * and ns represent significant ($p < 0.05$) and non-significant ($p \geq 0.05$) differences, respectively (Tukey's multiple comparison test). All of the statistical parameters and analysis results including sample size *n* and *p* values are provided in Supplementary Data 2. Source data are provided as a Source Data file.

For this purpose, we employed FAM-Xpep-TATs for preparing homodimer-depleted specimens. Since all experiments were performed at expression levels of ≈1 OR spot/μm^2, the percentages of the OR protomers existing as homodimers are 10–20% without any addition, 3.2–4.4% after the addition of FAM-Xpep-TATs, and 10–17% after the agonist addition, which is decreased to 2.9–8.4% after the further addition of FAM-Xpep-TATs (see the column of 1 copy/μm^2 in Table 3).

First, we examined OR internalization, which was monitored by using the membrane-impermeable fluorescence quencher, Mn(III) meso-tetra(4-sulfonatophenyl)porphine (Mn^{3+}-TSP). This quencher only suppresses fluorescence emission from the SNAP-Surface 549 dye on the SNAPf-OR on the cell surface, but not that in the cytoplasm[71]. Accordingly, by subtracting the signal intensity after the quencher addition from that before the addition, we evaluated the percentages of OR molecules remaining in the PM (Fig. 6a and Supplementary Fig. 8a).

The time courses of the decrease in the numbers of ORs remaining in the PM during 35 min (due to their internalization) were examined in both the presence and absence of 0.2 μM agonists and ≈3 μM Xpeps in the cytoplasm (Fig. 6a, b; Table 2 and Supplementary Data 2). All the time-course data obtained under various conditions could be fitted with a single exponential function plus a constant. The constant provides the OR fraction whose internalization is undetectable by the 35-min observations, and the exponential decay constant provides the residency lifetime in the PM for the OR component whose internalization was detectable by this observation scheme (Table 2 and Supplementary Data 2). Such high-levels of quantification were made possible by our observations of ORs with single-molecule sensitivities.

Without agonist, the three ORs all exhibited non-internalized fractions in the range of 91–95% (for an observation period of 35 min). The internalized molecules found during the 35 min observations showed characteristic dwell lifetimes (inverse of internalization rates). The homodimer-blocking peptides, FAM-Xpep-TATs, significantly reduced homodimers, but did not significantly affect the OR internalization (Fig. 6b and Table 2).

The addition of agonists employed in this investigation greatly increased the fractions of detectable internalizations and the internalization rates for all three engaged ORs (Fig. 6b and Table 2), whereas their effects on dimerization are complex (after agonist additions, the percentage of KOR protomers existing as homodimers decreases from 20 to 10%, while those for MOR and DOR increase from 10 to 16% and 10 to 17%, respectively; Table 3). FAM-Xpep-TATs added together with agonists reduced the homodimer percentages to the levels close to those after the addition of FAM-Xpep-TATs in the absence of agonists (Table 3), but had only slight (for engaged KOR) or no (for engaged MOR and DOR) additional effects on internalization (Fig. 6b and Table 2).

The lack of effect (or only the slight effect) of FAM-Xpep-TATs on the agonist-induced OR internalization (counted by protomer numbers) might be induced because the internalization rate of homodimers as an internalization unit (two protomers together as a homodimer) might become about half of that of monomers or the processes involving GRK and β-arrestin 2[27,72–74] might remove the ORs bound by these proteins from the monomer-dimer equilibrium in the bulk PM. However, due caution in the interpretation of these data is required because the Xpep-bound C-terminal domain might inhibit or enhance the interaction with GRK and β-arrestin 2 (for the Gqi5 binding, see the next subsection).

In addition to CHO-K1 cells, T24 cells were employed for these experiments because the expression level of β2-arrestin in T24 cells is higher than that in CHO-K1 cells[75,76], and thus T24 cells might undergo more active internalization. However, T24 cells exhibited internalization behaviors quite similar to those of CHO-K1 cells (Fig. 6b; Supplementary Table 2 and Supplementary Data 2).

Xpeps modulate KOR and DOR signals

To further elucidate the biased responses of OR monomers and homodimers, we examined the downstream signaling via the G protein. Since the direct estimation of Gi-mediated signals for Gi-coupled GPCRs has been difficult under the OR expression level of ≈1 copy/μm^2 employed for single-molecule imaging, we observed the Ca^{2+} mobilization mediated by the artificial G protein Gqi5 (Fig. 6c–e), which has been quite well established[77–81]. We showed that this method provides similar agonist dose dependences for suppressing forskolin-induced cAMP accumulation for DAMGO (for MOR) and SNC80 (for DOR) in cells expressing far higher levels of ORs (Supplementary Fig. 1a–c and Methods)[79,80,82].

The addition of the homodimer-blocking FAM-Xpep-TATs alone, which induces monomerization of ORs, did not induce any detectable Ca^{2+} mobilization (Fig. 6f and Table 2). In contrast, the respective agonists readily triggered Ca^{2+} mobilization. The effects of the homodimer-blocking peptides on the agonist-induced Ca^{2+} mobilization were complex (both FAM-Xpep-TATs and mGFP-Xpeps produced similar effects for all three ORs). In cells expressing KOR, MOR, or DOR, the homodimer-blocking peptides (OR monomerization) enhanced, did not affect, and reduced the agonist-induced Ca^{2+} mobilization, respectively (Fig. 6f and Table 2). These results indicate that KOR and DOR monomers trigger higher and lower signals than their respective homodimers, whereas MOR monomers and homodimers induce the downstream signals at similar levels (without influencing the agonist-induced internalization of all ORs; Fig. 6b). In short, homodimerization suppresses the ligand-induced signaling in KOR but enhances it in DOR. The DOR results were confirmed by a cAMP assay using cells with high DOR expression (5–10 fluorescent spots/μm^2), which demonstrated that 2 μM Dpep-TAT suppressed the SNC80-induced Gi-mediated lowering of the cAMP level in cells (Supplementary Fig. 8b–d).

As shown in the previous subsection, the internalization counted by the protomer number is very similar for OR monomers and homodimers (Fig. 6a, b). Therefore, we conclude that the biased response capability of DOR homodimers is stronger than DOR monomers, that of KOR homodimers is weaker than KOR monomers, and the biased response capability is the same for MOR homodimers and monomers.

Discussion

In this work, we developed new, simple single-molecule imaging methods to quantitatively evaluate the dimer dissociation rate constant (k_{off}), the dimer-monomer dissociation equilibrium constant (K_{D}), and the dimer formation rate constant (k_{on}) for any membrane molecules in the two-dimensional membrane of live cells. This was achieved by developing theories for analyzing single-molecule colocalization duration data, which enabled rigorous extraction of k_{off} (Supplementary Note 1), and by applying the PCCFs of two-color fluorescent spots in single-molecule images, which provide methods to measure K_{D} with enhanced sensitivity and ease (Supplementary Note 2). k_{on} can be evaluated as $k_{\mathrm{off}}/K_{\mathrm{D}}$.

In previous investigations of membrane molecule interactions and dimerizations, the results tended to be qualitative and often dominated by the employed expression levels. To enhance the qualities of studies on molecular dimerizations and interactions in the PM, which are particularly important for understanding receptor function regulations, measurements of these three parameters for membrane-impregnated molecules (K_{D}, k_{on}, and k_{off}) are indispensable. However, this has been technically challenging, and to date only two reports have provided the values for these critical constants, as listed in Table 1.

Our newly developed methods allow these constants for membrane molecules to be determined more readily, paving the way for a broad range of researchers to quantitatively examine membrane-molecule interactions and dimerizations in the PM. When combined with the knowledge of molecular expression levels (number densities in the PM), K_{D} yields the equilibrium distribution of dimers versus monomers (Fig. 2c), and k_{on} and k_{off} will reveal how quickly the dimers form and disassemble. Together, these advances represent a major step forward for studies of molecular interactions in the PM.

These three critical parameters describing the homodimer-monomer dynamic equilibrium have been determined for the OR. This was done for the three classical ORs before and after the addition of a representative agonist for each OR (Table 3). The results unequivocally demonstrated that the three classical ORs all form transient metastable homodimers and OR homodimers represent substantial proportions of functional entities at local number densities over 0.3 copies/μm^2 at 37 °C, both before and after the agonist binding (Table 3 and Fig. 2c). It is very possible that local number densities are higher in the PM areas with more signaling significance, which would imply an even higher functional significance of KOR and DOR homodimers and oligomers.

A previous single-molecule imaging study of neurotensin receptor 1, a GPCR, in reconstituted membranes containing only this receptor and a phospholipid revealed that it forms homodimers. This result demonstrated that neurotensin receptor 1 homodimerization occurs without the involvement of any other proteins[21] and suggested that ORs might also form homodimers without the involvement of other molecules. Meanwhile, another study showed that a specific agonist is required to induce MOR dimerization[14].

Importantly, all of these homodimers are forming and dispersing continually, with lifetimes shorter than 0.2 s at 37 °C (Fig. 1d). When the homodimers dissociate into monomers, they will again form homodimers with the same and other partner molecules. How the limited dimer fractions and lifetimes modulate the downstream signaling and internalization is extensively discussed in the companion paper (Fig. 8c and related main text)[39].

A previous biochemical study detected DOR homodimers and identified the aa sequence responsible for DOR dimerization[9]. Our DOR results agree with these previous findings, and further clarified that all three ORs, including DOR, undergo rapid interconversions between monomers and homodimers within a few seconds even at expression levels of about 1 copy/μm^2, and virtually all of the OR molecules experience existences as homodimers and monomers during this period. Our results provide a dynamic view of OR homodimerization with a clear quantitative basis.

Meanwhile, at apparent variance with our results, previous single-molecule examinations demonstrated that MOR and KOR tend to exist as monomers even at 20 °C, when expressed at levels between 0.1 and 0.3 copies/μm^2 [2,14,36]. Since we employed somewhat higher number densities of ≈1 OR spot/μm^2, corresponding to ≈1.8 OR molecular copies/μm^2 (caption to Fig. 2c), the dimerization event number per unit time in our study could be greater by a factor of 30–300. Therefore, the discrepancy might simply be due to the use of OR number densities lower than the sensitivity limit (very few homodimers exist in an image). This underscores the critical importance of evaluating the homodimer-monomer dissociation equilibrium constant K_D, rather than simply trying to detect homodimers[41].

Approximately two to five times greater K_D values (weaker molecular binding) compared to those found here have been reported for KOR[35] and MOR[28] at RT and 20 °C, respectively, while almost all measurements in this report have been performed at 37 °C. For comparison, we performed measurements for KOR at 20 °C and found that, as expected, the K_D increased with a concomitant increase in k_{off} and decrease in k_{on}. However, the extents of the changes are quite limited, and our KOR K_D value and the previously reported value differed by a factor of about six. The reason for this difference is unclear. The SEM/mean ratio in our case is 20%, whereas it is 47% in the previous report, which suggests that our estimate might be more accurate.

The agonist-bound KOR exhibited a greater K_D value (fewer dimers), whereas the agonist-bound MOR and DOR exhibited smaller K_D values (more dimers) (Table 3), although these results might vary depending on the particular agonist[9,14]. For example, the DOR agonists DADLE, DSLET, and DPDPE were previously found to induce fewer homodimers[9], but in the present research, another DOR agonist, SNC-80, increased the homodimer fraction, suggesting that the dimerization propensity depends on each agonist. We only examined one agonist for each OR subtype, because an extensive examination of the agonist effects on OR homodimerization is beyond the scope of the present work.

Specific 9-26 residue amino-acid sequences in the near-C-terminal cytoplasmic domains, which lack sequence similarities among the three ORs, are involved in the distinct homodimerizations of all three classical ORs (Figs. 3b, c, and 4), and do not participate in heterodimerization (Figs. 2a and 3a in the companion paper)[42]. Three experimental approaches supported this conclusion about OR homodimerization: (1) deletion mutants (Fig. 3b, c), (2) point mutants (Fig. 3d), and (3) two ways of adding the peptides with sequences found by approaches (1) and (2) (Fig. 4). Together, our conclusions have been strengthened, as each approach has its own shortcomings.

In the homo-interactions of C-terminal domains, in addition to localized interactions such as electrostatic, π-π, and π-S interactions, intrinsically disordered structures of the C-terminal regions, might be important for homodimerization (Supplementary Figs. 4 and 5)[61]. The enhancement of homodimerization by the intrinsically disordered region might not be due to liquid-liquid phase separation, but rather to its ability to flexibly adopt various structures, bringing several specific but weak binding sites into positions and orientations for optimal interactions.

In the literature on homo- and hetero-dimerization of GPCRs, including ORs, the TM domains have been proposed or found to be responsible for homodimerization[21,26,55,56,66,67]. In the present study, we found that TM1^{MOR} indeed binds to MOR and blocks MOR homodimerization (Fig. 5b, c, and e), suggesting the involvement of TM1^{MOR} in MOR homodimerization. However, we further found that it also binds to DOR, blocking DOR homodimerization (Fig. 5b, c, and e), which suggests that TM1^{MOR} is involved in MOR-DOR heterodimerization (see the companion paper for details)[42]. These results suggest that TM1^{MOR} interaction with ORs is likely to be quite non-specific, although it will not be involved in MOR-KOR heterodimerization (Fig. 5e). Furthermore, we found that Xpeps failed to reduce the OR homo-colocalization indexes to the level of a monomer control molecule TM^{LDLR}. Therefore, we propose that TM1^{MOR} would enhance both MOR-MOR and MOR-DOR dimers in less specific manners, whereas the cytoplasmic C-terminal domain interactions provide the specificities for OR homodimerization.

Other TM domains and extracellular domains that were not tested here might further facilitate OR dimerization. For example, in MOR homodimerization, TM5/TM6[56,83], as well as TM1,2,H8/TM5,6 and TM1,2,H8/TM5[26], have been identified as key interfaces and were proposed to form asymmetric dimers[26]. In DOR homodimerization, TM4/4 and TM4/TM5 were proposed as key interfaces forming symmetric dimers[67,84]. Notably, symmetric and asymmetric binding modes might be interchangeable[85].

Under the expression levels employed in this study (≈1 copy/μm^2), we rarely found homo-oligomers greater than dimers. However, due to the presence of secondary binding between TM domains, homo-oligomers might form at the much higher concentrations in the PM. Meanwhile, hetero-oligomers greater than dimers would occur at higher number densities (see Fig. 8 in the companion paper)[42], like the case of heterotetramer formation from the MOR homodimer and galanin Gal1 receptor homodimer[83].

Using FAM-Xpep-TATs for preparing homodimer-depleted specimens, we examined the biased responses of OR monomers and homodimers by evaluating their signaling and internalization. Interestingly, the internalization counted by the protomer number is very similar for monomers and homodimers in the cases of all three ORs (Fig. 6a, b). This result suggests that the internalization rate of homodimers as a unit might become about half of that of monomers. The signaling function of DOR homodimers is greater than that of monomers, but KOR homodimers exhibited less signaling ability than monomers, while MOR-induced signals are unaffected by homodimerization (in short, homodimerization suppresses the ligand-induced signaling of KOR, enhances that of DOR, and does not affect that of MOR). Since internalization does not depend on homodimerization state, the signaling functions of OR homodimers and monomers found here directly represent the signal's biased level of OR homodimers and monomers.

Due caution is required for the interpretation of these results, because the ORs' monomerization totally depended on FAM-Xpep-TATs in this study (we did not use point or deletion mutants, which would be interesting future study targets). It is possible that these results might be induced by the interfering effect of the bound peptide on the binding of Gqi5 to ORs (Gqi5's binding site to ORs is the same as the original Gαi) because the Gi binding to class A GPCRs involves various intracellular domains[73,74,86–89]. However, since the Halo-tag protein bound to the C-termini of ORs does not affect OR-induced Ca^{2+} responses[42] and since the peptide binding induces distinct effects on the three ORs, we think it is likely that the effects of homodimer blocking peptides on the agonist-induced Ca^{2+} signals can be interpreted based on their effects on OR monomerization.

Furthermore, these results suggest that the homodimer-blocking peptide-TATs could be used as reagents (drugs) to enhance or suppress the agonist-induced G-protein-biased cellular responses for KOR and DOR, respectively, without affecting their internalization (Fig. 6b). However, note that these results are correct only for the employed agonists, and the results would be agonist-dependent.

These homodimer blocking peptides could serve as the basis for designing modulators and potentiators in opioid therapy to enhance the efficacy and suppress side effects such as tolerance development, particularly for the opioids targeting KOR and DOR. The development of agonists for favorable biased signaling is important[90–93], but the modulation of the OR homodimerization would provide another means to produce biased signaling. Since the Xpep-TATs are soluble and yet membrane-permeable (Fig. 4e-h) and thus they are likely to pass the blood-brain barrier, they could be readily delivered via intravenous injections or nasal sprays. In addition, Xpep-TATs would not compete with agonist binding because they bind to the cytoplasmic C-terminal domains. Taken together, our findings reported here have greatly extended our knowledge of ORs' metastable homodimers and their formation mechanisms and functions, which can inform novel GPCR drug development strategies of modulating homodimerization.

Methods

cDNA construction

All of the newly generated cDNA constructs and other constructs obtained from outside sources, including gifts and constructs from commercial sources, were sequenced to examine their exact DNA sequences. The cDNA encoding rat MOR tagged with GFP was a gift from Dr. R. Schülz of the University of Münich, Germany[94]. The cDNA encoding rat KOR and DOR was a gift from Dr. Hiroshi Takeshima of the Kyoto University[95]. The mCherry was a gift from Prof. R. Y. Tsien of the University of California San Diego[96]. The cDNA encoding CD47 was a gift from Eric C. Brown of Genentech[97]. The cDNA encoding CD28 was a gift from Simon J. Davis of University of Oxford[98]. The cDNAs encoding SNAPf and mGFP (A206K) were obtained from New England Biolabs and Clontech, respectively. To generate plasmids for expressing SNAPf-ORs in CHO-K1 cells, the tag protein SNAPf was attached to the N-terminus of the ORs, an additional signal sequence of interleukin 6 was attached to the N-terminus of the tag protein, and a 21 amino-acid linker (SGGGSGG x 3) was inserted between the ORs and the tag protein. The deletion and point mutants of ORs were generated using a Q5® Site-Directed Mutagenesis Kit (NEB, Cat #E0554). The detailed cDNA information is included in Supplementary Data 1.

Cell culture, transfection, and microscope observations

CHO-K1 cells (Dainippon Pharma), GM3-null CHO-K1 cells (gift from Prof. K. Furukawa of Chubu University)[70], T24 cells[99] and HEK293 cells (Thermo Fisher Scientific) were confirmed free of mycoplasma contamination by MycoAlert (Lonza). CHO-K1 cells, GM3-null CHO-K1 cells, and T24 cells were routinely cultured in Ham's Nutrient Mixture F12 (Sigma-Aldrich) supplemented with 10% (v/v) fetal bovine serum (FBS, Life Technologies), 100 units/mL penicillin (Sigma-Aldrich), and 0.1 mg/mL streptomycin at 37 °C under a 5% CO_2 atmosphere. For cDNA transfections for single-molecule tracking studies of ORs (exhibiting 0.5 ~ 1 fluorescent spots/μm^2), approximately 5×10^6 cells were mixed with 200 ng OR cDNA plasmids in 100 μL transfection buffer, and electroporation was performed according to the manufacturer's instructions (4D-Nucleofector, Lonza; SF Cell Line solution and program for CHO-K1 and T24 cells). For cDNA transfections for Ca^{2+} mobilization and cAMP assays with Gqi5 and cAMPinG1, approximately 2×10^5 cells were mixed with 1 μg cDNA plasmids encoding Gqi5 and cAMPinG1 in 100 μL transfection buffer. The transfected cells were seeded in glass-base dishes (35 mm in diameter with a 12 mm diameter glass window, 0.15 mm-thick glass; Iwaki, Tokyo; 2×10^5 cells/dish) and cultured for 24–48 h before fluorescence microscopy observations. All microscope observations were performed at 37 °C by placing the entire microscope, except for the far ends of the excitation arms and the detection arms, in a home-built microscope environment chamber made with thermo- and electric-field-insulating plastic sheets and equipped with four heating circulators (SKHO-112-OT, Kokensya, Tokyo, Japan). The Ham's F12 medium used for microscope observations was free of sodium bicarbonate and phenol red, and buffered with 2 mM N-[tris(hydroxymethyl)methyl]-2-aminoethanesulfonic acid (TES, Sigma-Aldrich) at pH 7.4 (called Ham's F12 observation medium).

HEK293A cells (Thermo Fisher Scientific) used for the GloSensor cAMP assay were maintained in Dulbecco's Modified Eagle Medium (DMEM; Nissui Pharmaceutical), supplemented with 5% FBS (Gibco, Thermo Fisher Scientific), 100 units/mL penicillin (Sigma-Aldrich), 100 μg/mL streptomycin (Gibco) and 2 mM L-glutamine (Gibco). Cells were cultured at 37 °C under a 5% CO_2 atmosphere. Transfection was performed with a polyethylenimine (PEI) solution (Polyethylenimine "Max", Polysciences). Typically, HEK293A cells were seeded in a 6-well culture plate at a density of $2–3 \times 10^5$ cells/mL in 2 mL of medium and cultured for one day. A transfection solution was prepared by combining a plasmid solution diluted in 100 μL of Opti-MEM (Gibco, Thermo Fisher Scientific) with 100 μL of Opti-MEM containing 5 μL of 1 mg/mL PEI (Opti-MEM−PEI). The transfected cells were further incubated for 24 hours before use in assays.

Cell treatments with agonists and FAM-Xpep-TATs

U-50488, DAMGO, and SNC-80 (Sigma-Aldrich), agonists for KOR, MOR and DOR, respectively, were applied to the cells in the same way. The agonists were dissolved in DMSO (2 mM), and then diluted with Hanks' balanced salt solution (HBSS, Nissui) buffered with 2 mM TES at pH 7.4 (T-HBSS), at a final concentration of 200 μM. The agonist solution (1 μl) was added to the cells in 1 ml Ham's F12 observation medium (a final concentration of 200 nM) at 37 °C.

For the cellular incorporation of FAM-Xpep-TATs (custom-synthesized by Cosmo-Bio), the cells were first incubated with 150 μM pyrenebutyrate (Sigma-Aldrich) in T-HBSS at 37 °C for 5 min, and then 2 mM FAM-Xpep-TAT in T-HBSS was added at a final peptide concentration of 20 μM[64]. After an incubation at 37 °C for 10 min, the cells were washed three times with T-HBSS, and then fresh Ham's F12 observation medium was added to the cells. The presence of FAM-Xpep-TAT in the cytoplasm was confirmed by the addition of the membrane-impermeable quencher, trypan blue[100].

Cholesterol depletion and replenishment

Partial depletion of cholesterol was achieved by incubating the cells in 4 mM methyl-β-cyclodextrin (MβCD, Sigma Aldrich: 332615) at 37 °C for 30 min. Replenishment of cholesterol was performed by incubating the cholesterol-depleted cells in 10 mM MβCD-cholesterol complex (1:1 mol/mol; Sigma Aldrich: C3045) at 37 °C for 10 min[101].

Fluorescence labeling of ORs

The SNAPf-tagged wild-type and mutant ORs expressed in the PM (SNAPf tag located at the extracellular N-terminus) were covalently conjugated by simultaneously incubating the cells with two fluorescent SNAP ligands, SNAP-Surface 549 (New England Biolabs) and SNAP-CF660R (Shinsei Kagaku), both at 300 nM, in the growth medium at 37 °C in the CO_2 incubator for 30 min. The cells were washed three times with fresh medium (5 min incubation each time), and then the Ham's F12 observation medium was added.

The labeling efficiency (the percentage of the SNAPf-tag protein labeled with the fluorescent SNAP ligand) was determined in the following way, by employing five proteins: monomeric TM proteins (CD47, TM^{LDLR}, and MOR's aa 1–70 sequence linked to the N-terminus of TM^{LDLR}) expressed at a spot number density of ≈1 spot/μm^2, and MOR and MOR's Δ358-382 mutant (monomeric mutant developed in this study) expressed at a spot number density of <0.1 spot/μm^2. Each protein was tagged with a SNAPf-tag protein at the N-terminus and with mGFP (for CD47) or monomeric StayGold (mSG) at the C-terminus (for the other four proteins)[102]. The details of the determination are described in Supplementary Fig. 1d-f.

After labeling, in general, the populations of cells exhibiting expression levels of 1.0 ± 0.5 fluorescent spots/μm^2, and those with greater or lower expression than this level were each about one-third of the cells found in the dish (lower expression here includes the cells that do not show any fluorescence labeling even under single-molecule imaging conditions).

Single molecule fluorescence imaging

Fluorescently labeled ORs expressed in the bottom PM (the PM facing the coverslip) at fluorescent-spot number densities of 0.5 ± 0.25 spots/μm^2 for each color (SNAP-Surface 549 and SNAP-CF660R; total spot number densities of 1.0 ± 0.5 spots/μm^2; for conciseness, we describe the number densities as ≈1 spot/μm^2 throughout this report) were observed at the level of single molecules at 37 °C, using a home-built objective lens-type TIRF microscope constructed on an inverted microscope (Olympus IX-83), with a 100x, 1.49 numerical aperture (NA) objective lens, optimized for the present research based on the instrument used previously[48,103]. ORs tagged with fluorescent probes were excited with TIR illumination using the following power densities: SNAP-Surface 549 at 561 nm (Coherent OBIS 561-100 LS) at 0.35 μW/μm^2; and SNAP-CF660R at 642 nm (Omicron LuxXPlus 640-140) at 0.52 μW/μm^2. The dual-color images were separated by a dichroic mirror ZT640rdc-UF3 (Chroma) and projected into two detection arms with band-pass filters of 575-625 nm (ET600/50 m; Chroma) for the SNAP-Surface 549 dye and 662.5–737.5 nm (ET700/75 m; Chroma) for the SNAP-CF660R dye. In some experiments using mGFP-Xpeps and FAM-Xpep-TATs, an additional detection arm equipped with a dichroic mirror ZT561rdc-UF3 (Chroma) and a band-pass filter of 500.0–550.0 nm (ET525/50 m; Chroma) was employed. The fluorescence signal in each channel was first detected and amplified by a two-stage microchannel-plate image intensifier (C9016-02MLP24; Hamamatsu Photonics), and the intensified image was projected onto the scientific CMOS camera (C11440-22CU; Hamamatsu Photonics), operated at 30 Hz, which was synchronized with the same intensifier-camera set(s) placed on another detection arm. The image sequences in each channel were superimposed after correction for spatial distortions, as described previously[48]. The positions (x and y coordinates) of all of the observed single fluorescent-molecules were determined by an in-house computer program, as described previously[104].

Evaluating colocalization durations and dimer dissociation rate constant

The colocalization of two fluorescent molecules was defined as the event where two fluorescent spots, representing these molecules, become localized within 200 nm of each other, as described previously[41,48]. Briefly, in single-color experiments using SNAP-Surface 549 (Supplementary Fig. 2a and b), a spatial cross-correlation analysis was employed[41]. Using this method, we found that when two fluorescent spots, each representing a single molecule of SNAP-Surface 549, are located close together, the threshold distance for discriminating one or two spots occurred at 200 nm in the present experimental set up. Using this definition, colocalized trajectories were obtained and colocalization durations were estimated.

In the simultaneous two-color single fluorescent-molecule tracking approach, which is extensively used in this study, we also selected 200 nm as the threshold distance for determining colocalization of fluorescent spots in two different colors. This is based on the analyses of (1) sensitivity to detect colocalization (next paragraph), (2) avoiding incidental oligomers greater than dimers (Supplementary Fig. 2f), and (3) precisions of the determined homodimer lifetimes (Supplementary Table 3 related to Supplementary Note 1).

In simultaneous two-color single fluorescent-molecule tracking experiments, using the dye pairs of SNAP-Surface 549 and SNAP-CF660R, the distance between the two molecules was directly measured from the locations (x, y-positions) of each molecule (with different colors). Even when examining pairs of different-colored molecules that are known to be truly associated, the probability of scoring the two molecules as associated is limited by the sum of the localization accuracies of each molecule and the accuracies of superimposing the two images (σ). Based on the method developed previously[48] and the accuracies determined here, we found that, for truly associated molecules, the probability of scoring the two molecules as associated increases to 86.6% - 98.8% (1.5x – 2.5x of σ) when using the criterion that the molecules lie within 200 nm of each other. Therefore, we used this criterion as the definition of colocalization in simultaneous two-color single-molecule observations. This distance of 200 nm coincided with the definition of colocalization in single-color experiments. Due to this coincidence, in the present research, we defined the colocalization of two fluorescent molecules as the event where the two fluorescent spots representing these molecules become localized within 200 nm from each other.

Each time we found a green-magenta pair located within 200 nm (colocalization), we measured the duration in which their distances remained within 200 nm (colocalized duration) (for the results obtained by using two dye molecular species with different excitation/emission wavelengths, we call them green and magenta probes/movies for convenience in this report). After obtaining the colocalization durations for all of the colocalization events, we generated a histogram (distribution) of colocalization durations. The distribution of incidental colocalization durations was obtained by superimposing the magenta image sequences with the 180-degree rotated (doubly flipped) green image sequences (Supplementary Fig. 2d). For the precise analysis of these histograms, we first produced cumulative histograms and fitted them with a single exponential function ($C_0 - C_1\exp[-t/\tau_1]$) or the sum of two exponential functions ($C_0 - C_1\exp[-t/\tau_1] - C_2\exp[-t/\tau_2]$). The choice of the number of exponentials (including the cases of the sum of three exponential functions) was made based on Akaike's and Bayesian information criteria (they always agreed). Based on these functions, the functions describing the original histograms were derived and overlaid on the histograms.

First, we found that the distribution of incidental colocalization durations could be fitted by a single exponential function, with a time constant representing the incidental colocalization lifetime $\tau_{\rm inci}$. Second, the distribution of colocalization durations was obtained for correctly superimposed magenta and green image sequences. This distribution could be fitted by the sum of two exponential decay functions (τ_1 and τ_2; $\tau_1 < \tau_2$,). These results are consistent with the theory developed here that predicts the distribution of colocalization durations based on the diffusion equation (Supplementary Note 1). Since τ_1 was almost the same as $\tau_{\rm inci}$ (Fig. 1e), following the theory developed in Supplementary Note 1, τ_2 provided the homodimer lifetime (this value has to be corrected for the trackable duration lifetimes of the two fluorescent probes, to obtain $k_{\rm off}$).

The trackable duration lifetime is obtained from the distribution of trajectory lengths of SNAPf-MOR expressed in CHO-K1 cells labeled with SNAP-Surface 549 or SNAP-CF660R, which would represent how long single molecules can be continuously tracked under the influences of photobleaching and loss of signals due to blinking and the entrance of the molecules into the PM areas located farther from the PM. The distributions could be fitted as single exponential functions providing trackable duration lifetimes ($\tau_{\rm track}$'s) of 16.3 ± 1.2 s ($n = 500$) for SNAP-Surface 549 and 7.8 ± 0.6 s ($n = 400$) for SNAP-CF660R bound to SNAPf-MOR expressed in CHO-K1 cells observed at 30 Hz (Supplementary Fig. 2g). The correction was made by using the equation:

$$\tau(\text{corrected}) = [\tau(\text{observed})^{-1} - \tau_{\text{track}}(\text{dye})^{-1} - \tau_{\text{track}}(\text{dye2})^{-1}]^{-1}.$$

$$k_{\text{off}} \text{ is calculated as } 1/\tau(\text{corrected}).$$

Evaluating the colocalization index

For the quantitative evaluation of the extent of colocalization (representing both the frequency and lifetime of colocalization events) in simultaneous two-color single-molecule imaging movies, we defined a parameter called the colocalization index. This analysis method is essentially based on a pair cross-correlation analysis[51], and the detailed method used in this research is explained in Supplementary Fig. 2c-e and 3.

Evaluating dimer-monomer dissociation equilibrium constant, K_D

K_D was determined by fitting the experimental PCCF using the number density of fluorescent spots obtained from the movie and the fluorescence labeling efficiencies of 0.66 for SNAP-Surface 549 and 0.61 for SNAP-CF660R, as well as the fitting parameters, K_D and the precision of overlaying two-color movies plus single-molecule localizations for two fluorescent probes, as described in Supplementary Note 2. The numbers of movies are provided in Supplementary Data 2, along with other statistical parameters.

Monte-Carlo simulations

For the detailed method for Monte-Carlo simulations to examine the theory to obtain K_D from the pair cross-correlation function (PCCF) (Supplementary Note 2), see the Supplementary Methods to Supplementary Fig. 3.

The colocalization index depends on the number density of fluorescent spots in the PM. In the present experimental observations, we selected the cells exhibiting fluorescent spot number densities in the PM of 0.5 ± 0.25 spots/μm^2 for each color (SNAP-Surface 549 and SNAP-CF660R; total spot number densities of 1.0 ± 0.5 spots/μm^2; for conciseness, we describe the number densities as ≈1 spot/μm^2 throughout this report). These densities were found to be reasonable by the Monte-Carlo simulation results, which indicated that, for the K_D greater than 6.5 copies/μm^2, the colocalization index does not vary sharply in the number density range of 0.5–1.5 spots/μm^2 (refer to Supplementary Fig. 3c). At the same time, we developed the theory to evaluate the dimer-monomer dissociation equilibrium constant K_D from the PCCF and the total number of spots in the image (refer to Supplementary Note 2).

Prediction of the homodimer structure of DOR's C-terminal cytoplasmic domain

We used the Chai Discovery web https://lab.chaidiscovery.com/ interface to predict the homodimer structures for the C-terminal cytoplasmic domains[105]. Such prediction software is difficult to use for dimers of transmembrane proteins, because in the absence of the membrane, their highly ranked predicted structures are all dominated by the transmembrane domains. However, when we tested the homodimerization of three full length ORs without constraints, the highly ranked predicted homodimer structures of all three ORs exhibited short membrane proximal α helices with high confidence, corresponding to the well-conserved amino acid sequence of DENFKRCFRXXC. This region appears to be stabilized by π-sulphur and π-π interactions.

Therefore, in the second prediction round, we only examined the homodimerization of the C-terminal cytoplasmic domains and introduced three contact type constraints to align the alpha helices of both chains (A and B), by fixing the distances between the residues phenylalanine F4 (chain A) with F4 (chain B) as 5 Å, F8 (chain A) and cysteine C12 (chain B) as 4 Å, and finally C12 (chain A) and F8 (chain B) as 4 Å (see the conserved sequence shown in the previous paragraph). The predicted structures for the C-terminal cytoplasmic domains of MOR and KOR, but not that of DOR, exhibited extensive α helices, which is inconsistent with the predicted disorder scores shown in Supplementary Fig. 4b, and therefore, we decided to only focus on the prediction for DOR's C-terminal cytoplasmic domain homodimer structure. The resulting highest-ranked model was visualized as cartoons highlighted with the stick-models, using PyMol 3.1 by Schrödinger.

Confocal imaging to study the effects of mGFP-Xpeps and FAM-Xpep-TATs on cells stably expressing ORs

CHO-K1 cells stably expressing ORs were transfected with mGFP-Xpeps. The cells were identified by the incubation with NucSpot Live 650 Nuclear Stain (Biotium), according to the protocol recommended by the manufacturer. After three washes with the complete medium, it was replaced with the Ham's F12 observation medium. The incorporation of the FAM-Xpep-TATs in the cells was performed as described in a previous subsection "Cell treatments with agonists and FAM-Xpep-TATs". Confocal fluorescence images were acquired on the same microscope station used for single-molecule imaging at 37 °C, which is equipped with a spinning-disc confocal unit (Yokogawa, CSU-W1).

GFP and FAM were excited at 488 nm and detected through a 525–550 nm band pass filter. The NucSpot Live 650 was excited at 642 nm and detected through a 662.5–737.5 nm long pass filter. The concentrations of cytoplasmic mGFP-Xpep and FAM-Xpep-TAT were evaluated using calibration curves, obtained by observing the purified EGFP protein (BioVision) and FAM-Xpep-TATs dissolved in Ham's F12 observation medium at various concentrations, with a focus at 5 μm above the cover-glass surface (Supplementary Fig. 6b).

Ca^{2+} mobilization assay

Since the OR expression level varies from cell to cell, the signaling process must be observed at the level of individual cells. The ORs are coupled to the inhibitory trimeric G protein Gi, which induces the decrease of the cytoplasmic cAMP concentration by inhibiting adenylyl cyclase. However, using the cells with low OR expression levels employed for single-molecule observations (≈1 fluorescent spot/μm^2), the decrease of the cytoplasmic cAMP levels in individual cells from those in non-stimulated state was impossibly difficult to measure. Meanwhile, the increase of the cytoplasmic Ca^{2+} concentrations by the PLCβ activated by the Gq signaling pathway could be measured in individual cells[79,80,82]. Therefore, in this assay, Gαq was modified so that OR could be coupled to Gαq. Namely, the C-terminal five amino-acid sequence of Gαq, ECGLY, was replaced with that of Gαi2, DCGLF (this chimeric protein is called Gqi5), because the Gα protein binds to the specific GPCR by way of its short C-terminal sequence[81]. Therefore, we generated the CHO-K1 cell line stably expressing Gqi5, had it express the OR, and then observed the cytoplasmic Ca^{2+} mobilization upon agonist addition, using the Ca^{2+}-sensitive dyes (Fig. 6c–f and Supplementary Fig. 1b). This method of using Gqi5 has been widely employed in the research of ORs[82] and other Gi-coupled GPCRs[80]. Briefly, CHO-K1 cells stably expressing Gqi5 were generated and transfected with the cDNAs encoding the non-tagged and SNAPf-linked ORs. The Ca^{2+}-sensitive dyes Fluo-4 AM (Dojindo) and Rhod-3 AM (Thermo Fisher Scientific) were employed. Rhod-3 was used for the experiments with mGFP-Xpeps and FAM-Xpep-TATs, and Fluo-4 was used for the experiments that did not employ these homodimer-blocking reagents. These AM dyes were incorporated in the cell, according to the manufacturers' recommendations, using the following solutions: for Fluo-4, 4.6 μM Fluo-4 AM in T-HBSS containing 1.25 mM Probenecid (Dojindo) and 0.04 % (w/v) Pluronic F127 (Dojindo), and for Rhod-3, 10 μM Rhod-3 AM in T-HBSS containing 2.5 mM Probenecid and 1× PowerLoad™ (Thermo Fisher Scientific). These loading solutions (2 ml) were added to the cells and incubated in the dark at 37 °C for 30 min, and then the cells were washed three times with T-HBSS.

For the observations of the Ca^{2+} mobilization downstream of the SNAPf-tagged ORs, we selected cells expressing SNAPf-tagged ORs bound by SNAP-Surface 549 (or SNAP-CF660R for experiments using Rhod-3) at number densities of ≈1 fluorescent spot/μm^2 in the basal PM, using single-molecule detection (TIRF illumination) in the 561 nm channel (642 nm channel when we employed Rhod-3). These cells were then observed by epifluorescence illumination using the

488-nm channel to monitor the Fluo-4 signal (561-nm channel to observe the Rhod-3 signal and 488-nm channel for mGFP-Xpeps and FAM-Xpep-TATs). Agonist stimulation was performed by adding the DMSO solutions of agonists at a final concentration of 200 nM. The Ca^{2+} mobilization was parametrized by using $[F_{Max}\text{-}F_b]/F_b$, where F_{Max} is the maximal Fluo-4 or Rhod-3 signal intensity within 75 s after the addition of the stimulants and F_b is the baseline intensity (Fig. 6e). To determine the saturation levels of the fluorescence signal intensity at higher concentrations of Ca^{2+}, 1 μM (final concentration) ionomycin (Wako) was added (which would increase the intracellular Ca^{2+} concentration to that outside the cells [1.3 mM]). The Fluo-4 and Rhod-3 image sequences were analyzed using the ImageJ software.

For the comparison of the functions of the SNAPf-ORs with those of the non-tagged ORs, we hoped to compare the cells expressing the SNAPf-ORs at the levels of ≈1 spot/μm^2 in the basal PM with the cells expressing the non-tagged ORs at levels comparable to or higher than those of SNAPf-ORs, because the cells expressing the non-tagged ORs should serve as the positive controls. For this purpose, the expression levels of non-tagged ORs were monitored by using cells transfected with the cDNA linking the non-tagged OR sequence to the mCherry sequence via the self-cleavable 2 A linker sequence (mCherry-2A-OR). This way, mCherry is released from the OR into the cytoplasm at the ER, and the non-tagged OR is then transported to the PM. The expression of non-tagged OR was detected by the presence of mCherry in the cytoplasm using the epi-illumination at 561 nm (sensitivities much lower than single-molecule imaging, showing the presence of rather high concentrations of mCherry). Therefore, the expression of the non-tagged OR used in this study is considered higher than that of SNAPf-ORs.

GloSensor cAMP assay

$G\alpha_i$-mediated inhibition of cAMP production was measured using an in-house-modified GloSensor cAMP assay, as described previously[106,107]. HEK293 cells were transfected with a mixture of 200 ng of opioid receptor-encoding plasmid and 500 ng of Glo-22F cAMP biosensor-encoding plasmid. After 24 h of incubation, the transfected cells were harvested with 0.53 mM EDTA-containing PBS, centrifuged at 190 × g for 5 min, and suspended in 1 mL HBSS containing 0.01% BSA (fatty-acid-free grade; SERVA) and 5 mM HEPES (pH 7.4) (assay buffer). The cell suspension was dispensed in a white 96-well plate at a volume of 40 μL per well and then loaded with 10 μL of 10 mM *D*-luciferin potassium solution (FujiFilm Wako Pure Chemical) diluted in the assay buffer. After a 2 h incubation in the dark at room temperature, baseline luminescence was measured using a SpectraMax L plate reader (Molecular Devices). Subsequently, 10 μL of 6 × ligand diluted in the assay buffer, or the assay buffer alone (vehicle) was manually added. Cells were treated with 10 μM forskolin (FujiFilm Wako Pure Chemical), an adenylyl cyclase activator, together with a titrated concentration of DAMGO or SNC80. Luminescence was recorded at 60 s intervals for 20 min at room temperature. The luminescence counts from 16 to 20 min after ligand addition were averaged and normalized to the initial counts. Concentration–response curves were generated by dividing the luminescence change at each agonist concentration by that of the vehicle condition.

The agonist-induced signals determined by the GloSensor cAMP assay were fitted to a four-parameter sigmoidal concentration-response curve, using the GraphPad Prism 10 software (GraphPad Software). The fitted concentration–response curve was used to obtain the pEC_{50} ($-\log_{10} EC_{50}$) values.

cAMPinG1 cAMP assay

For establishing CHO-K1 cells used for cAMPinG1 cAMP assay, which stably expressed tagged OR at levels 5–10 times higher than those used for single-molecule imaging, we transfected 2×10^5 CHO-K1 cells with 1 μg DOR cDNAs, and cloned the transfected cells. CHO-K1 cells stably expressing SNAPf-DOR were transfected with the cDNAs encoding cAMPinG1[108]. Approximately 2×10^5 cells were mixed with ≈1 μg cAMPinG1 plasmids in 100 μL transfection buffer, and electroporation was carried out with a 4D-Nucleofector electroporation apparatus, according to the manufacturer's instructions (4D-Nucleofector, Lonza; SF Cell Line solution and program for CHO-K1 cells). The transfected cells were seeded in glass-base dishes and cultured for 24–48 h before fluorescence microscopy observations. All microscope observations were performed at 37 °C.

For the cAMP inhibition assay, cells expressing SNAPf-DOR labeled with SNAP-Surface 549 on the basal PM were selected using TIRF microscopy with 561 nm excitation. Time-lapse imaging of cAMPinG1 was performed every 30 s with 100 ms 405 nm and 488 nm laser illuminations (sequential 100 ms × 2). After 5 min of baseline imaging, forskolin (Sigma-Aldrich) was added to a final concentration of 7 μM. Following 10 min of further imaging, SNC-80 was added to a final concentration of 50 nM, and imaging continued for an additional 10 min. Image sequences were analyzed as previously described[108].

Software and statistical analysis

The microscope station that combined a single-molecule imaging system and a super-resolution confocal microscope was controlled by in-house LabVIEW2018-based software, and the single-molecule movie acquisitions were performed using the MCR software (Hamamatsu Photonics) for Windows. All statistical analyses for in vitro experiments were performed with Tukey's multiple comparison test except for the analysis of the colocalization lifetime data, which was performed with the Brunner-Munzel test, using RStudio 1.2.1335 for Windows. P values less than 0.05 were considered statistically significant. The confocal images were processed and analyzed using ImageJ for Windows. Curve fitting was performed by OriginPro 2019b for Windows. The simulation study was performed using the in-house software based on MATLAB 2019a for Windows. Statistical parameters, including the numbers of movies, cells, and independent replicates as well as p values, are provided in Supplementary Data 2. We used the Chai Discovery web https://lab.chaidiscovery.com/ interface to predict the homodimer structures for the C-terminal cytoplasmic domains. The resulting highest-ranked model was visualized as cartoons highlighted with the stick-models, using PyMol 3.1 by Schrödinger. Figures and videos were edited using Photoshop CC 2021, Illustrator CC 2021 (Adobe).

Reporting summary

Further information on research design is available in the Nature Portfolio Reporting Summary linked to this article.

Data availability

Source data are provided with this paper. All data necessary to support the conclusions of this study are provided in the main text, main figures, Supplementary Information, and Source data file. Raw movies and images used for quantification are available from the corresponding authors upon request. Source data are provided with this paper.

Code availability

Custom-written computer codes for data collection and analysis are available at Zenodo with entry number 17160485[109].

References

1. Darcq, E. & Kieffer, B. L. Opioid receptors: drivers to addiction?. *Nat. Rev. Neurosci.* **19**, 499–514 (2018).
2. Valentino, R. J. & Volkow, N. D. Untangling the complexity of opioid receptor function. *Neuropsychopharmacology* **43**, 2514–2520 (2018).

3. Grimes, J. et al. Plasma membrane preassociation drives β-arrestin coupling to receptors and activation. *Cell* **186**, 2238–2255.e2220 (2023).
4. Schmid, C. L. et al. Bias factor and therapeutic window correlate to predict safer opioid analgesics. *Cell* **171**, 1165–1175.e1113 (2017).
5. Che, T. & Roth, B. L. Molecular basis of opioid receptor signaling. *Cell* **186**, 5203–5219 (2023).
6. Hauser, A. S., Attwood, M. M., Rask-Andersen, M., Schiöth, H. B. & Gloriam, D. E. Trends in GPCR drug discovery: new agents, targets and indications. *Nat. Rev. Drug Discov.* **16**, 829–842 (2017).
7. Spangler, S. & Bruchas, M. R. Tuning biased GPCR signaling for physiological gain. *Cell* **171**, 989–991 (2017).
8. Bag, N. et al. Lipid-based and protein-based interactions synergize transmembrane signaling stimulated by antigen clustering of IgE receptors. *Proc. Natl. Acad. Sci. USA.* **118**, e2026583118 (2021).
9. Cvejic, S. & Devi, L. A. Dimerization of the delta opioid receptor: implication for a role in receptor internalization. *J. Biol. Chem.* **272**, 26959–26964 (1997).
10. He, L., Fong, J., von Zastrow, M. & Whistler, J. L. Regulation of opioid receptor trafficking and morphine tolerance by receptor oligomerization. *Cell* **108**, 271–282 (2002).
11. Fujita, W., Gomes, I. & Devi, L. A. Revolution in GPCR signalling: opioid receptor heteromers as novel therapeutic targets: IUPHAR review 10. *Br. J. Pharmacol.* **171**, 4155–4176 (2014).
12. Gomes, I. et al. A role for heterodimerization of μ and δ opiate receptors in enhancing morphine analgesia. *Proc. Natl Acad. Sci. USA.* **101**, 5135 (2004).
13. Jordan, B. A. & Devi, L. A. G-protein-coupled receptor heterodimerization modulates receptor function. *Nature* **399**, 697–700 (1999).
14. Möller, J. et al. Single-molecule analysis reveals agonist-specific dimer formation of μ-opioid receptors. *Nat. Chem. Biol.* **16**, 946–954 (2020).
15. Ilien, B. et al. Pirenzepine promotes the dimerization of muscarinic M1 receptors through a three-step binding process. *J. Biol. Chem.* **284**, 19533–19543 (2009).
16. Liu, J. et al. Biased signaling due to oligomerization of the G protein-coupled platelet-activating factor receptor. *Nat. Commun.* **13**, 6365 (2022).
17. Gomes, I. et al. Identification of a μ-δ opioid receptor heteromer-biased agonist with antinociceptive activity. *Proc. Natl. Acad. Sci. Usa.* **110**, 12072 (2013).
18. Waldhoer, M. et al. A heterodimer-selective agonist shows in vivo relevance of G protein-coupled receptor dimers. *Proc. Natl. Acad. Sci. Usa.* **102**, 9050 (2005).
19. Kasai, R. S., Fujiwara, T. K., Kusumi, A. Metastable GPCR dimers trigger the basal signal by recruiting G-proteins. *bioRxiv*, 2020.2002.2010.929588 (2020).
20. He, S. Q. et al. Facilitation of μ-Opioid receptor activity by preventing δ-opioid receptor-mediated codegradation. *Neuron* **69**, 120–131 (2011).
21. Dijkman, P. M. et al. Dynamic tuneable G protein-coupled receptor monomer-dimer populations. *Nat. Commun.* **9**, 1710 (2018).
22. Ferré, S., Ciruela, F., Woods, A. S., Lluis, C. & Franco, R. Functional relevance of neurotransmitter receptor heteromers in the central nervous system. *Trends Neurosci.* **30**, 440–446 (2007).
23. Fribourg, M. et al. Decoding the signaling of a GPCR heteromeric complex reveals a unifying mechanism of action of antipsychotic drugs. *Cell* **147**, 1011–1023 (2011).
24. George, S. R., O'Dowd, B. F. & Lee, S. P. G-protein-coupled receptor oligomerization and its potential for drug discovery. *Nat. Rev. Drug Discov.* **1**, 808–820 (2002).
25. Navarro, G. et al. Evidence for functional pre-coupled complexes of receptor heteromers and adenylyl cyclase. *Nat. Commun.* **9**, 1242 (2018).
26. Meral, D. et al. Molecular details of dimerization kinetics reveal negligible populations of transient μ-opioid receptor homodimers at physiological concentrations. *Sci. Rep.* **8**, 7705 (2018).
27. Asher, W. B. et al. Single-molecule FRET imaging of GPCR dimers in living cells. *Nat. Methods* **18**, 397–405 (2021).
28. Gentzsch, C. et al. Selective and wash-resistant fluorescent dihydrocodeinone derivatives allow single-molecule imaging of μ-opioid receptor dimerization. *Angew. Chem. Int. Ed.* **59**, 5958–5964 (2020).
29. Erbs, E., Faget, L., Veinante, P., Kieffer, B. L. & Massotte, D. In vivo neuronal co-expression of mu and delta opioid receptors uncovers new therapeutic perspectives. *Receptors Clin. Investig.* **1**, (2014).
30. Erbs, E. et al. A mu–delta opioid receptor brain atlas reveals neuronal co-occurrence in subcortical networks. *Brain Struct. Funct.* **220**, 677–702 (2015).
31. Pierre, F. et al. Morphine-dependent and abstinent mice are characterized by a broader distribution of the neurons co-expressing mu and delta opioid receptors. *Neuropharmacology* **152**, 30–41 (2019).
32. DiCello, J. J. et al. Mu and delta opioid receptors are coexpressed and functionally interact in the enteric nervous system of the mouse colon. *Cell. Mol. Gastroenterol. Hepatol.* **9**, 465–483 (2020).
33. George, S. R. et al. Oligomerization of mu- and delta-opioid receptors: generation of novel functional properties. *J. Biol. Chem.* **275**, 26128–26135 (2000).
34. Wang, D., Sun, X., Bohn, L. M. & Sadée, W. Opioid receptor homo- and heterodimerization in living cells by quantitative bioluminescence resonance energy transfer. *Mol. Pharmacol.* **67**, 2173–2184 (2005).
35. Cechova, K. et al. Kappa but not delta or mu opioid receptors form homodimers at low membrane densities. *Cell. Mol. Life Sci.* **78**, 7557–7568 (2021).
36. Drakopoulos, A. et al. Investigation of inactive-state κ opioid receptor homodimerization via single-molecule microscopy using new antagonistic fluorescent probes. *J. Med. Chem.* **63**, 3596–3609 (2020).
37. Rogacki, M. K. et al. Dynamic lateral organization of opioid receptors (kappa, mu(wt) and mu(N40D)) in the plasma membrane at the nanoscale level. *Traffic* **19**, 690–709 (2018).
38. Calebiro, D. et al. Single-molecule analysis of fluorescently labeled G-protein–coupled receptors reveals complexes with distinct dynamics and organization. *Proc. Natl. Acad. Sci. USA* **110**, 743 (2013).
39. Hern, J. A. et al. Formation and dissociation of M1 muscarinic receptor dimers seen by total internal reflection fluorescence imaging of single molecules. *Proc. Natl. Acad. Sci. USA.* **107**, 2693 (2010).
40. Kasai, R. S., Ito, S. V., Awane, R. M., Fujiwara, T. K. & Kusumi, A. The class-A GPCR dopamine D2 receptor forms transient dimers stabilized by agonists: detection by single-molecule tracking. *Cell. Biochem. Biophys.* **76**, 29–37 (2018).
41. Kasai, R. S. et al. Full characterization of GPCR monomer-dimer dynamic equilibrium by single molecule imaging. *J. Cell. Biol.* **192**, 463–480 (2011).
42. Zhou, P. et al. Single-molecule characterization of opioid receptor heterodimers reveals soluble μ-δ dimer blocker peptide alleviates morphine tolerance. *Nat. Commun.* https://doi.org/10.1038/s41467-025-64695-2 (2025).
43. Hernanz-Falcón, P. et al. Identification of amino acid residues crucial for chemokine receptor dimerization. *Nat. Immunol.* **5**, 216–223 (2004).
44. Jastrzebska, B. et al. Disruption of rhodopsin dimerization with synthetic peptides targeting an interaction interface. *J. Biol. Chem.* **290**, 25728–25744 (2015).

45. McMillin, S. M., Heusel, M., Liu, T., Costanzi, S. & Wess, J. Structural basis of M3 muscarinic receptor dimer/oligomer formation. *J. Biol. Chem.* **286**, 28584–28598 (2011).
46. Petersen, J. et al. Agonist-induced dimer dissociation as a macromolecular step in G protein-coupled receptor signaling. *Nat. Commun.* **8**, 226 (2017).
47. Pan, Y. X. Expression of opioid receptors in mammalian cell lines. In: *opioid research: Methods and Protocols* (ed Pan Z. Z.). Humana Press (2003).
48. Koyama-Honda, I. et al. Fluorescence imaging for monitoring the colocalization of two single molecules in living cells. *Biophys. J.* **88**, 2126–2136 (2005).
49. Koyama-Honda, I. et al. High-speed single-molecule imaging reveals signal transduction by induced transbilayer raft phases. *J. Cell. Biol.* **219**, (2020).
50. Kusumi, A., Sako, Y. & Yamamoto, M. Confined lateral diffusion of membrane receptors as studied by single particle tracking (nanovid microscopy). Effects of calcium-induced differentiation in cultured epithelial cells. *Biophys. J.* **65**, 2021–2040 (1993).
51. Stone, M. B. & Veatch, S. L. Steady-state cross-correlations for live two-colour super-resolution localization data sets. *Nat. Commun.* **6**, 7347 (2015).
52. Fagan, R. R. et al. Selective targeting of mu opioid receptors to primary cilia. *Cell Rep.* **43**, 114164 (2024).
53. Evans, E. J. et al. Crystal structure of a soluble CD28-Fab complex. *Nat. Immunol.* **6**, 271–279 (2005).
54. Granier, S. et al. Structure of the δ-opioid receptor bound to naltrindole. *Nature* **485**, 400–404 (2012).
55. Huang, W. et al. Structural insights into µ-opioid receptor activation. *Nature* **524**, 315–321 (2015).
56. Manglik, A. et al. Crystal structure of the µ-opioid receptor bound to a morphinan antagonist. *Nature* **485**, 321–326 (2012).
57. Wu, H. et al. Structure of the human κ-opioid receptor in complex with JDTic. *Nature* **485**, 327–332 (2012).
58. Navarro, G. et al. Interactions between intracellular domains as key determinants of the quaternary structure and function of receptor heteromers. *J. Biol. Chem.* **285**, 27346–27359 (2010).
59. Mészáros, B., Erdős, G. & Dosztányi, Z. IUPred2A: context-dependent prediction of protein disorder as a function of redox state and protein binding. *Nucleic Acids Res.* **46**, W329–W337 (2018).
60. Erdős, G. & Dosztányi, Z. Analyzing protein disorder with IUPred2A. *Curr. Protoc. Bioinform.* **70**, e99 (2020).
61. Xhani, S. et al. Intrinsic disorder controls two functionally distinct dimers of the master transcription factor PU. *1. Sci. Adv.* **6**, eaay3178 (2020).
62. Kusumi, A., Tsunoyama, T. A., Suzuki, K. G. N., Fujiwara, T. K. & Aladag, A. Transient, nano-scale, liquid-like molecular assemblies coming of age. *Curr. Opin. Cell Biol.* **89**, 102394 (2024).
63. Sarkar, D. K., Sengupta, A., Zhang, C., Boyadjieva, N. & Murugan, S. Opiate antagonist prevents µ- and δ-opiate receptor dimerization to facilitate ability of agonist to control ethanol-altered natural killer cell functions and mammary tumor growth. *J. Biol. Chem.* **287**, 16734–16747 (2012).
64. Inomata, K. et al. High-resolution multi-dimensional NMR spectroscopy of proteins in human cells. *Nature* **458**, 106–109 (2009).
65. Grasberger, B., Minton, A. P., DeLisi, C. & Metzger, H. Interaction between proteins localized in membranes. *Proc. Natl Acad. Sci. USA.* **83**, 6258–6262 (1986).
66. Ferré, S. et al. G protein–coupled receptor oligomerization revisited: functional and pharmacological perspectives. *Pharmacol. Rev.* **66**, 413 (2014).
67. Johnston, J. M. et al. Making structural sense of dimerization interfaces of delta opioid receptor homodimers. *Biochemistry* **50**, 1682–1690 (2011).
68. Martínez-Muñoz, L. et al. Separating actin-dependent chemokine receptor nanoclustering from dimerization indicates a role for clustering in CXCR4 signaling and function. *Mol. Cell* **70**, 106–119.e110 (2018).
69. Harding, P. J. et al. Constitutive dimerization of the G-protein coupled receptor, neurotensin receptor 1, reconstituted into phospholipid bilayers. *Biophys. J.* **96**, 964–973 (2009).
70. Yamashiro, S. et al. Substrate specificity of beta 1,4-N-acetylgalactosaminyltransferase in vitro and in cDNA-transfected cells. GM2/GD2 synthase efficiently generates asialo-GM2 in certain cells. *J. Biol. Chem.* **270**, 6149–6155 (1995).
71. Keppler, A., Pick, H., Arrivoli, C., Vogel, H. & Johnsson, K. Labeling of fusion proteins with synthetic fluorophores in live cells. *Proc. Natl Acad. Sci. USA.* **101**, 9955–9959 (2004).
72. Smith, J. S. et al. Noncanonical scaffolding of Gαi and β-arrestin by G protein–coupled receptors. *Science* **371**, eaay1833 (2021).
73. Wess, J., Oteng, A. B., Rivera-Gonzalez, O., Gurevich, E. V. & Gurevich, V. V. β-arrestins: structure, function, physiology, and pharmacological perspectives. *Pharmacol. Rev.* **75**, 854–884 (2023).
74. Zhou, X. E. et al. Identification of phosphorylation codes for arrestin recruitment by G protein-coupled receptors. *Cell* **170**, 457–469.e413 (2017).
75. Ménard, L. et al. Synergistic regulation of beta2-adrenergic receptor sequestration: intracellular complement of beta-adrenergic receptor kinase and beta-arrestin determine kinetics of internalization. *Mol. Pharmacol.* **51**, 800–808 (1997).
76. Kallifatidis, G. et al. β-arrestins regulate stem cell-like phenotype and response to chemotherapy in bladder cancer. *Mol. Cancer Ther.* **18**, 801–811 (2019).
77. Dratz, E. A. et al. NMR structure of a receptor-bound G-protein peptide. *Nature* **363**, 276–281 (1993).
78. Gleixner, J. et al. Illuminating neuropeptide Y Y4 receptor binding: fluorescent cyclic peptides with subnanomolar binding affinity as novel molecular tools. *ACS Pharmacol. Transl. Sci.* **7**, 1142–1168 (2024).
79. Yokoyama, T., Kato, N. & Yamada, N. Development of a high-throughput bioassay to screen melatonin receptor agonists using human melatonin receptor expressing CHO cells. *Neurosci. Lett.* **344**, 45–48 (2003).
80. Han, Y., Moreira, I. S., Urizar, E., Weinstein, H. & Javitch, J. A. Allosteric communication between protomers of dopamine class A GPCR dimers modulates activation. *Nat. Chem. Biol.* **5**, 688–695 (2009).
81. Conklin, B. R., Farfel, Z., Lustig, K. D., Julius, D. & Bourne, H. R. Substitution of three amino acids switches receptor specificity of Gqα to that of Giα. *Nature* **363**, 274–276 (1993).
82. Camarda, V., Calo', G. Chimeric G proteins in fluorimetric calcium assays: experience with opioid receptors. In: *Calcium Signaling Protocols* (eds Lambert D. G., Rainbow R. D.). Humana Press (2013).
83. De Oliveira, P. A. et al. Preferential Gs protein coupling of the galanin Gal(1) receptor in the µ-opioid-Gal(1) receptor heterotetramer. *Pharmacol. Res.* **182**, 106322 (2022).
84. Provasi, D., Johnston, J. M. & Filizola, M. Lessons from free energy simulations of delta-opioid receptor homodimers involving the fourth transmembrane helix. *Biochemistry* **49**, 6771–6776 (2010).
85. Di Marino, D., Conflitti, P., Motta, S. & Limongelli, V. Structural basis of dimerization of chemokine receptors CCR5 and CXCR4. *Nat. Commun.* **14**, 6439 (2023).

86. Hauser, A. S. et al. GPCR activation mechanisms across classes and macro/microscales. *Nat. Struct. Mol. Biol.* **28**, 879–888 (2021).
87. Zhou, Q. et al. Common activation mechanism of class A GPCRs. *Elife* **8**, (2019).
88. Mafi, A., Kim, S. K. & Goddard, W. A. 3rd. Mechanism of β-arrestin recruitment by the μ-opioid G protein-coupled receptor. *Proc. Natl. Acad. Sci. USA.* **117**, 16346–16355 (2020).
89. Koehl, A. et al. Structure of the μ-opioid receptor–Gi protein complex. *Nature* **558**, 547–552 (2018).
90. Che, T., Dwivedi-Agnihotri, H., Shukla, A. K. & Roth, B. L. Biased ligands at opioid receptors: current status and future directions. *Sci. Signal.* **14**, eaav0320 (2021).
91. Violin, J. D., Crombie, A. L., Soergel, D. G. & Lark, M. W. Biased ligands at G-protein-coupled receptors: promise and progress. *Trends Pharmacol. Sci.* **35**, 308–316 (2014).
92. Manglik, A. Molecular basis of opioid action: from structures to new leads. *Biol. Psychiatry* **87**, 6–14 (2020).
93. De Neve, J. et al. Comprehensive overview of biased pharmacology at the opioid receptors: biased ligands and bias factors. *RSC Med. Chem.* **12**, 828–870 (2021).
94. Schulz, R., Wehmeyer, A. & Schulz, K. Opioid Receptor Types Selectively Cointernalize with G Protein-Coupled Receptor Kinases 2 and 3. *J. Pharmacol. Exp. Ther.* **300**, 376 (2002).
95. Fukuda, K., Kato, S., Mori, K., Nishi, M. & Takeshima, H. Primary structures and expression from cDNAs of rat opioid receptor δ- and μ-subtypes. *FEBS Lett.* **327**, 311–314 (1993).
96. Shaner, N. C. et al. Improved monomeric red, orange and yellow fluorescent proteins derived from Discosoma sp. red fluorescent protein. *Nat. Biotechnol.* **22**, 1567–1572 (2004).
97. Lindberg, F. P., Gresham, H. D., Schwarz, E. & Brown, E. J. Molecular cloning of integrin-associated protein: an immunoglobulin family member with multiple membrane-spanning domains implicated in alpha v beta 3-dependent ligand binding. *J. Cell. Biol.* **123**, 485–496 (1993).
98. James, J. R., Oliveira, M. I., Carmo, A. M., Iaboni, A. & Davis, S. J. A rigorous experimental framework for detecting protein oligomerization using bioluminescence resonance energy transfer. *Nat. Methods* **3**, 1001–1006 (2006).
99. Fujiwara, T. K. et al. Development of ultrafast camera-based single fluorescent-molecule imaging for cell biology. *J. Cell. Biol.* **222**, e202110160 (2023).
100. Cowen, T., Haven, A. J. & Burnstock, G. Pontamine sky blue: a counterstain for background autofluorescence in fluorescence and immunofluorescence histochemistry. *Histochemistry* **82**, 205–208 (1985).
101. Suzuki, K. G. et al. Transient GPI-anchored protein homodimers are units for raft organization and function. *Nat. Chem. Biol.* **8**, 774–783 (2012).
102. Ando, R. et al. StayGold variants for molecular fusion and membrane-targeting applications. *Nat. Methods* **21**, 648–656 (2024).
103. Murakoshi, H. et al. Single-molecule imaging analysis of Ras activation in living cells. *Proc. Natl. Acad. Sci. Usa.* **101**, 7317 (2004).
104. Fujiwara, T. K. et al. Confined diffusion of transmembrane proteins and lipids induced by the same actin meshwork lining the plasma membrane. *Mol. Biol. Cell.* **27**, 1101–1119 (2016).
105. Chai Discovery teamBoitreaud, J. et al. *bioRxiv*, 2024.10.10.615955 (2024).
106. Tatsumi, M. et al. Identification of Gα12-vs-Gα13-coupling determinants and development of a Gα12/13-coupled designer GPCR. *Sci. Rep.* **14**, 11119 (2024).
107. Kawakami, K. et al. Heterotrimeric Gq proteins act as a switch for GRK5/6 selectivity underlying β-arrestin transducer bias. *Nat. Commun.* **13**, 487 (2022).
108. Yokoyama, T. et al. A multicolor suite for deciphering population coding of calcium and cAMP in vivo. *Nat. Methods* **21**, 897–907 (2024).
109. Zhou, P. et al. Single-molecule methods for characterizing receptor dimers reveal metastable opioid receptor homodimers that induce functional modulation, Zenodo, https://doi.org/10.5281/zenodo.17160485, (2025).

Acknowledgements

We thank Profs. H. Takeshima of Kyoto University, R. Schülz of the University of Münich, R. Y. Tsien of the University of California San Diego, Simon J. Davis of the University of Cambridge, and Michiyuki Matsuda of Kyoto University, for their kind gifts of cDNAs encoding rat KOR and DOR, that encoding rat MOR, that encoding mCherry, that encoding CD28, plasmids of pPBpuro and pCMV-mPBase, respectively. We also thank Ms. Irina Meshcheryakova for technical help in preparing the cDNAs. This work was supported in part by Japan Society for the Promotion of Science (JSPS) Grants-in-Aid for Scientific Research (Kiban A to A.K. [21H04772] and A.I. [21H04791], Kiban S to A.K. [16H06386], Kiban B to T.K.F. [20H02585, 24K01310], M.Y. [24K01982], and M.S. [JP23H02782], Kiban C to R.S.K. [17K07333], Wakate B to R.S.K. [26870292], Wakate to T.A.T. [21K15058] and T.Y. [24K18240], Kaitaku to A.I. [24K21281], and Challenging Exploratory Research to T.K.F. [18K19001] and A.K. [22K19334]), a Grant-in-Aid from the Ministry of Education, Culture, Sports, Science and Technology of Japan (MEXT) for Transformative Research Areas (A) to T.K.F. (21H05252) and M.Y. (24H01266), Transformative Research Areas (B) to M.S. (JP24H00861), a JST grant ACT-X to T.A.T. (JPMJAX211B) and T.Y. (JPMJAX211K), FOREST to A.I. (JPMJFR215T), and Moonshot to A.I. (JPMJMS2023), an AMED grant Brain/MIND 2.0 to M.S. (JP24wm0625119) and OIST Proof of Concept Program Technology Pioneer Fellowship to P.Z. (R11_61). WPI-iCeMS of Kyoto University is supported by the World Premiere Research Center Initiative (WPI) of MEXT.

Author contributions

P.Z., R.S.K., and A.K. conceived and formulated the project. A.K., T.A.T., T.K.F., and P.Z. developed the simultaneous dual-color single-molecule tracking station. P.Z., T.A.T., R.S.K., and A.K. designed biological experiments, and P.Z., with help from T.A.T., performed virtually all of the biological and microscopic experiments. T.K.F. developed and improved the in-house image analysis software. S.P. developed the theory for evaluating the k_{off} from the single-molecule experimental data (Supplymentary Note 1). K.M.H., T.A.T., and A.K. developed the colocalization index method, and T.A.T., Z.K., and A.K. developed the theory for linking the PCCF to the dimer dissociation equilibrium constant and performed Monte-Carlo simulations to prove the theory (Supplymentary Note 2). A.A. performed the OR sequence analysis to detect intrinsically disordered regions and obtained the predicted structure of the homodimer of DOR's C-terrminal cytoplasmic domain. T. Y. and M. S. prepared the cNDA of cAMPinG1 for cAMP assay, and P.Z., with help from M.S., T.Y., and T.A.T., conducted a cAMPinG1-based cAMP assay. R.K., M.Y., and A.I. performed cAMP assays to examine OR-induced signals. A.K., P.Z., and T.A.T. wrote the manuscript, and all authors discussed the results and participated in the manuscript revisions.

Competing interests

P.Z. and A.K. are inventors on a patent application (patent pending) for Xpeps and Xpep-TATs described in this study. The remaining authors declare no competing interests.

Additional information

Supplementary information The online version contains supplementary material available at https://doi.org/10.1038/s41467-025-64694-3.

Correspondence and requests for materials should be addressed to Peng Zhou or Akihiro Kusumi.

Peer review information *Nature Communications* thanks Tijana Jovanović-Talisman who co-reviewed with Carina LimaVittorio Limongelli who co-reviewed with Stefano Raniolo; Sergi Ferre and the other, anonymous, reviewer(s) for their contribution to the peer review of this work. A peer review file is available.

Reprints and permissions information is available at http://www.nature.com/reprints

Publisher's note Springer Nature remains neutral with regard to jurisdictional claims in published maps and institutional affiliations.

Open Access This article is licensed under a Creative Commons Attribution-NonCommercial-NoDerivatives 4.0 International License, which permits any non-commercial use, sharing, distribution and reproduction in any medium or format, as long as you give appropriate credit to the original author(s) and the source, provide a link to the Creative Commons licence, and indicate if you modified the licensed material. You do not have permission under this licence to share adapted material derived from this article or parts of it. The images or other third party material in this article are included in the article's Creative Commons licence, unless indicated otherwise in a credit line to the material. If material is not included in the article's Creative Commons licence and your intended use is not permitted by statutory regulation or exceeds the permitted use, you will need to obtain permission directly from the copyright holder. To view a copy of this licence, visit http://creativecommons.org/licenses/by-nc-nd/4.0/.

© The Author(s) 2025